Hydrocarbon Gases from Giant Piston Cores in the Northern Gulf of Mexico: Results from the IMAGES VIII/PAGE 127 cruise of the RV Marion Dufresne, July, 2002

Thomas D. Lorenson[1]
Jennifer A. Dougherty[1]
James G. Flocks[2]

[1]U.S. Geological Survey, 345 Middlefield Rd., MS-999, Menlo Park, California 94025 (tlorenson@usgs.gov)
[2]U.S. Geological Survey, 600 4th Street S., St. Petersburg, Florida 33701

Hydrocarbon Gases from Giant Piston Cores in the Northern Gulf of Mexico: Results from the IMAGES VIII/PAGE 127 cruise of the RV Marion Dufresne, July, 2002; *chapter 9* in *Winters, W.J., Lorenson, T.D., Paull, C.K., eds., 2005, Initial report of the IMAGES VIII/PAGE 127 gas hydrate and paleoclimate cruise on the RV* Marion Dufresne *in the Gulf of Mexico, 2-18 July 2002, U.S. Geological Survey Open-File Report 2004-1358.*

Abstract

Hydrocarbon gases and carbon dioxide (CO_2) extracted from sediment cores from the northern Gulf of Mexico in four distinct regions were studied to constrain the possible occurrence and source of gas that may form gas hydrate. Three sample types were analyzed; gas from dissociated gas hydrate, dissolved gas in sediment, and free gas evolved from sediment collected from gas voids in the core liner.

Gas hydrate was recovered in four cores from previously known venting sites about three to nine meters below the sea floor (mbsf), but was not found in adjacent basins. Gas hydrate samples were preserved for analysis from only one core, MD02-2569 in the thalweg of Mississippi Canyon within lease area MC802. The quality of the gas hydrate recovered was poor because the time for core recovery and sampling approached two hours. Methane, ranging from 95.0 to 99.5%, is the principal gas in the gas hydrate with concentrations of CO_2 ranging from 0.16% to 4.0%. Higher molecular weight hydrocarbon gases; ethane, propane and isobutane are found in concentrations exceeding 1000 parts per million (ppm) suggesting that both structure I and structure II gas hydrate are present.

Sediment collected near the summit of a 1 to 1.5-km diameter sea floor mound on Kane Spur within lease area MC853, (34-km east of MC802), contained visible oil and hydrocarbon gases of thermogenic origin. Sediment from MC802 contained some proportion of hydrocarbon gases of likely thermogenic origin, but at much lower concentrations than at MC853. Free gas from sediment at MC853 was also composed of mainly thermogenic hydrocarbons. Sediment gases from other areas (Tunica Mound, Bush Hill, and areas in and flanking Mississippi Canyon) were composed mainly of microbial methane with traces of thermogenic hydrocarbons.

Introduction

The northern Gulf of Mexico hosts numerous sea floor (<7m subbottom) occurrences of gas hydrate. The sea floor is dominated by salt-tectonic basin structures, high sedimentation rates (about 40 cm/kyr), and complex late Neogene stratigraphy with common sea floor failures. Natural oil and gas seeps are abundant, usually associated with fault conduits resulting in numerous hydrocarbon vents, often capped by gas hydrate when the seeps are within the hydrate stability zone. While gas hydrate is relatively common at the sea floor, the lack of bottom simulating reflections (BSR) on seismic records suggest that gas hydrate at depth is largely absent. Thus, it is unknown if there are significant gas hydrate accumulations in reservoir sediments away from faults. To address this question a cruise was conducted with the IMAGES (International Marine Past Global Changes Study) and PAGE (Paleoceanography of the Atlantic and Geochemistry) programs aboard the RV *Marion Dufresne* in July 2002 (Lorenson and others, 2002).

Eighteen giant piston cores, up to 38-m long, and four giant box cores up to 9-m long, were recovered along seismic reflection transects in widely different geologic environments in water depths ranging from 600-1300 m. The transects were designed to extend from known sea floor gas hydrate occurrences across the adjacent basin to background sediments away from any gas venting sites.

Dissolved and free gas in marine sediments is an important means of discriminating the gas source and relative concentration of hydrocarbon gas constituents. To this end, we measured the hydrocarbon gas content of sediments and used this data as proxies for methane and other hydrocarbon gas source discrimination, the general gas contents of the sediment, and the likely presence of gas hydrate that may dissociated during the core recovery process.

Methods

Field sampling

A variety of gas sample types were collected for this study: (1) Cored sediment (2) Free gas, and (3) Gas produced by controlled dissociation of gas hydrate samples.

Sediment destined for gas analysis were treated utilizing a procedure modified from Kvenvolden and Redden (1980): Cored sediment in a 5 cm interval was cut out, extruded from the core liner and sealed in a 500 mL metal can equipped with a septum. The sample was placed into a metal can equipped with a septum and weighed. The sample can was filled with water to the rim and 100 mL of water was removed. Two to three grams of sodium chloride salt was added as a bacterial growth inhibitor. The sample and water were sealed in the can leaving a 100 mL headspace. The samples were frozen in the upside-down position and shipped to our laboratory in Menlo Park, California for hydrocarbon gas analyses.

In the laboratory, the frozen samples were allowed to thaw in cans until they reached about 20 degrees C, then placed into a high-speed shaker and shaken for 5 minutes. The partitioned hydrocarbon gases in the headspace were analyzed. Gas sub-samples destined for carbon isotopic analyses were withdrawn by syringe and injected into a pre-evacuated 30 mL serum vial for shipment.

Free gas

Free gas samples were taken when visible signs of sediment extrusion were noticed during routine drilling of gas venting holes in the core liner. In such instances "mudworms" were commonly seen extruding from the holes. Gas was sampled by inserting a valve-tipped plastic syringe into the hole and allowing the gas to expand into the syringe. The gas in the syringe was injected into an evacuated 30-ml serum vial for transport to the laboratory and then analyzed by direct injection onto a gas chromatograph as described below.

Gas hydrate analyses

The system for measuring the gas and water content of dissociating gas hydrate consisted of a sample holder, a gauge block, a pressure gauge, and a manifold. The manifold has an interchangeable gas-sampling port with septum or a quick-connection to vacuum, a steel cylinder for collection of gas, and a pressure gauge. The device was first used on Deep Sea Drilling Program Leg 76 and a more complete description of it can be found in Kvenvolden and others, (1984). For each experiment, gas hydrate that was temporarily stored in liquid nitrogen was placed on aluminum foil and broken up. Pieces with minimal sediment were placed into the sample device previously cooled by liquid nitrogen. The system was sealed and the lower portion of the device was placed into a water bath. As the gas hydrate dissociated, pressure inside the device increased, then stabilized. After about ten minutes of stable pressure, the pressure and the temperature of the water bath were recorded. Dissociated gas was allowed to expand into the sample manifold and the pre-evacuated cylinder. Gas was sampled from the manifold and analyzed by gas chromatography. After gas sampling, the residual water and any sediment was weighed and their respective volumes calculated and subtracted from the volume of the reaction chamber. Gas volumes were calculated according to the ideal gas law at standard temperature and pressure (STP). Residual water was decanted after centrifugation, then sealed and refrigerated pending chlorinity measurements and isotopic analyses of the water.

Hydrocarbon gas composition determination

A Shimadzu GC-14A gas chromatograph equipped with a Chemipack C-18, 1.8 m. x 3.2 mm 80/100 mesh stainless steel column was used to measure C_1-C_8 hydrocarbon gases. The GC-14A is configured with a 1 mL, valve-actuated, sample loop for injection, and a flame ionization detector (FID) for gas detection. Samples were introduced by syringe at atmospheric pressure, and a minimum of 10 mL of gas was used to flush the injection loop. Run conditions were 35 degrees C for 1.5 minutes ramping up at 20 degrees/minute to 150 degrees C , and held. Helium was used as the carrier gas at a constant mass flow rate of 3 kg/cm^2. FID temperature was held at 150 degrees C.

Results are reported relative to the volume of cuttings or weight of core material from which the gases were extracted, i.e., microliters of gas per liter of wet sediment (μL/L). Gas concentration data are reported for a series of hydrocarbons given in order of elution (Table 1); methane (C_1), ethane (C_2), propane (C_3), isobutane (iC_4), normal butane (nC_4), neopentane ($neoC_5$), isopentane (iC_5), normal pentane (nC_5), 2,2 dimethylbutane ($2,2MC_4$), 2methylpentane ($2MC_5$), 3methylpentane ($3MC_5$), normal hexane (nC_6), normal heptane (nC_7) and methylcyclohexane (McC_6). Approximate detection limits for all hydrocarbon compounds are 0.05 parts per million by volume (ppm) corresponding to about 0.02μL/L.

CO_2 determination

Carbon dioxide (CO_2), concentrations were determined in laboratory with a Hewlett-Packard P-200 micro gas chromatograph equipped with a 4 m long by 50- m-diameter carboplot column. Run conditions were isothermal at 60 degrees C with a run time of 2 minutes. Helium carrier gas column head pressure was maintained at 1.25 bar. Compounds were detected with a micro-machined thermal conductivity detector. The approximate detection limit for CO_2 is about 0.5 μL/L. Concentrations of primary gases (nitrogen, oxygen, and argon) were not determined because the samples were exposed to air during recovery and packaging.

Hydrocarbon gas isotopic composition determination

Stable carbon isotope ratio determinations of C_1, C_2, C_3, iC_4, nC_4, nC_5, and CO_2 were made on a Continuous Flow–Isotope Ratio Mass Spectrometer (Finnigan MAT 252 GC-

CF-IRMS) at the School of Earth and Ocean Sciences (SOES), University of Victoria, Canada.

Samples were introduced by syringe into a Stanford Research Insturments gas chromatograph (GC) via a gas sample valve (loop volumes: 10, 100 or 200 μL). Analytes were separated at 40 degrees C on a 30 m GS-Q column (0.32 mm ID) with a carrier gas flow of 1.8 mL/min ultra-high purity helium. After gas partitioning on the GC, the gas then passes through a CuO/Pt microcombustion oven at 850 degrees C. This oven quantitatively converts the hydrocarbon gases to carbon dioxide and water. The combusted sample products were then passed through a Nafion™ tube to remove water from the combustion and any that may be in the carrier gas. The purified CO_2/He pulse was scaled by an open-split interface, and then transferred into the GC-C-IRMS. Isotope ratios are referenced to the conventional PDB standard through a known CO_2 isotope standard that is added at the open split to the sample runs several times during the analysis.

For stable carbon isotope ratio measurements on the sample CO_2, the gas was partitioned on the GC as above. The microcombustion oven was bypassed for the CO_2 measurements, but the gas stream was dried, split and measured by CF-IRMS in a manner similar to the light hydrocarbons.

Location

Sediment cores from the northern Gulf of Mexico in four distinct regions (fig. 1) were analyzed in this study: Tunica Mound, Pigmy Basin, Bush Hill, and the Mississippi Canyon area (Kane Spur and West Mississippi Canyon). Table 1 lists core locations that were analyzed for sediment gas concentration.

Tunica Mound

Garden Banks and Green Canyon are known for locally high sedimentation rates from 7 to 11 m/k.y. for the upper sedimentary section, extensive late Neogene salt deformation, and slope failures with mass-wasting along over steepened parts of the continental slope (Rowan and Weimer, 1998). Sediment ages in the upper 600-700 mbsf are likely no older than 0.5 m.y. in

the study area (Berryhill and others, 1987; Weimer and others, 1998). This region includes the Tunica Mound and Bush Hill coring sites.

The upper sedimentary section of the continental slope including Tunica Mound is characterized by layered and chaotic units that are faulted near basin edges, and by slope failures on basin flanks. Deformation is greater near salt structures and on over steepened slopes.

Downslope, well-layered sediments within 300 meter of the sea floor have many vertical acoustic "chimney" features, likely small faults, and are bounded by chaotic units directly below and above. The underlying chaotic unit has high reflectivity zones (HRZs) that are dispersed within chaotic stratal units, and similar to those in other slope basins at about the same depth Cooper and Hart (2003). These gas chimney features extend up from this chaotic unit to the overlying disrupted unit, which has low seismic amplitudes and evidence of faulting and sliding.

A transect of nine gravity and piston cores was taken along the southern flank of Tunica Mound verging toward but not entering the basin to the east (fig. 2). Tunica Mound is about 14 km^2 with a fault running through the southwest to northeast corners. The northwest side of the mound is uplifted in contrast to the southeast corner. The coring transect is about 7-km long at a subparallel angle to the fault in the southeast quadrant. Water depths along the transect range from 600 to 630 meters. All sites on the transect remain within the confines of the dome; however, the site to the NE enters the basin between Tunica Mound and Caddo Mound located to the east of Tunica Mound. Most of the gravity cores were taken on or near a subsidiary mound with features that indicate active

Table 1. Location of cores

Core ID	**Latitude**	**Longitude**	**Area Name**
MD02-2535	27.61983	92.24100	Tunica Mound
MD02-2537	27.61600	92.24867	Tunica Mound
MD02-2538GHF	27.61667	92.24717	Tunica Mound
MD02-2539	27.63967	92.19217	Tunica Mound
MD02-2541	27.63250	92.21233	Tunica Mound
MD02-2543G	27.61233	92.25550	Tunica Mound
MD02-2545G	27.61400	92.25167	Tunica Mound
MD02-2546	27.61567	92.24700	Tunica Mound
MD02-2553C2	27.18350	91.41667	Pigmy Basin
MD02-2554	27.78333	91.49900	Bush Hill Basin
MD02-2555	27.78317	91.48917	Bush Hill Basin
MD02-2556	27.78300	91.47750	Bush Hill Basin

MD02-2559	28.22250	89.08817	Kane Spur
MD02-2560	28.24333	89.15500	Kane Spur
MD02-2561	28.20517	89.02017	Kane Spur
MD02-2562	28.07983	89.14017	Kane Spur
MD02-2563	28.12333	89.13633	Kane Spur
MD02-2565	28.12350	89.13950	Kane Spur
MD02-2566	28.11917	89.10317	Kane Spur
MD02-2567	28.10017	89.01983	Kane Spur
MD02-2569	28.15217	89.47967	West Mississippi
MD02-2570	29.57100	89.68983	West Mississippi
MD02-2573GHF	28.15200	89.47983	West Mississippi

G= Gravity Core
GHF= Gravity Heat Flow Core
C2= Box Core

fluid flow including authigenic carbonate, sea floor relief, and seismic indications of gas. Piston cores were taken away from the sub-mound.

Pigmy and Orca Basins

Coring in Pigmy and Orca Basins was conducted by paleoceanograhic research interests on board (fig. 3) The basins presumably have similar depositional histories; however, Orca Basin has been covered by a seawater brine for some time causing an anoxic environment and preservation of organic matter. In contrast, Pigmy Basin has been subject to oxic conditions. Only one sample was analyzed from Pigmy Basin and none in Orca Basin.

Bush Hill

Coring commenced in the small basin just east of Bush Hill (fig. 4) along an east-west transect with cores about 2 km apart. Bush Hill itself has been extensively survey by numerous groups focusing on vent gas, gas hydrate, and chemosynthetic communities (MacDonald and others, 1989, 1994, 1996; Roberts and Carney, 1997; Roberts and others, 2001; Sassen and others, 1993, 1998, 1999a,b, 2001a,b, c). The Bush Hill sea floor feature is a fault-related seep mound at a water depth around 540 m that may have seismic attributes of a mud diapir. An antithetic fault at Bush Hill is structurally related to nearby growth faults that constitute the structural trap at Jolliet Field just a few

kilometers to the south (Cook and D'Onfro, 1991). The oil and gas at the Bush Hill site correlate with reservoirs at approximately 2–3 km depth in Jolliet Field (for example Kennicutt and others, 1988; Sassen and others, 2001a). Shallow sediment is under-consolidated hemipelagic mud with near-normal salinity (~38 ppt), high concentration of H_2S (as much as 20.3 μM/l), and high pH (8.3–9.0) (Aharon and Fu, 2000). Mounds of structure II gas hydrate outcrop on the sea floor and have been persistently observed since 1991 (Sassen and others, 2003).

Mississippi Canyon Region

Kane Spur

Cooper and Hart, (2003) recorded high-resolution seismic-reflection profiles across the east and west sides of the Mississippi Canyon. These areas are characterized by extreme sedimentation rates up to 15 20m/ky, pelagic drape and mass-wasting (Coleman and others, 1983) over the last 20 ky. The age of the sedimentary sections in the upper 600 -700 m is likely no older than late Pleistocene (Goodwin and Prior, 1989).

The most prominent feature on the east side of Kane Spur (fig. 5) is a large sea floor slide that is about 15 km wide and at least 15 km long, covering more than 225 km^2. Extensional faults are found at the head of the slide and a 1-2 km wide shear zone appears along the southwest edge of the slide. The slide exemplifies large-scale active slope failure common to the Mississippi Canyon area resulting from several causes including salt withdrawal and diapirism, deep- and shallow-extensional faulting, and gravity sliding (Cooper and Hart, 2003).

The subbottom is cut by two categories of faults: a suite of high-angle faults that converge with depth and extend off the bottom of the seismic-reflection record, and a set of faults that appear to be related to stratigraphic sliding within the upper sedimentary section. Cooper and Hart (2003) infer that the high-angle faults are rooted in deep-seated salt that is the principal driving mechanism for the sea floor slide. The shallow faults that sole out within a chaotic unit partly accommodate the slide motion that includes extension near the slide's head and compression near the toe.

Within the boundaries of the extensional subsidence zone, Cooper and Hart (2003) observed a chaotic stratigraphic unit that occurs with disrupted reflections and high reflectivity (HRZ). The gas hydrate stability field terminates within the HRZ. The top of the HRZ under the slide

lies at about 440 to 480 mbsf, is about 90 to130 m thick, and generally mimics the sea floor. The high reflectivity occurs mostly where reflections are discontinuous and chaotic. The unit can be traced regionally, but reflectivity is greatest under the slide and near large fault zones. During development of the Ursa Field, drilling along the southwest side of the slide encountered wet sands with overpressure shallow water flows and some gas from about 300 to 550 mbsf, (Eaton, 1999) such features are common in the northern Gulf of Mexico (MMS, 2001).

Mississippi Canyon

MC853 lease block diapiric structure

An oblong sea floor mound, perhaps a diapir, (1–1.5 km across) overlies a shallow salt body at the boundary of Mississippi Canyon lease blocks 852 and 853 referred to in this report as MC853. The MC853 sea floor mound is on a structural high along the extensional boundary of a salt withdrawal basin on the western flank of Kane Spur (Fig. 5). Allochthonous salt bodies occur at shallow depth in the sediment and have initiated major growth faults believed to serve as conduits for fluid migration to the sea floor from the subsurface petroleum system within salt withdrawal basins (Sassen and others, 1999a). An acoustic wipeout zone typical of fluid expulsion occurs below the mound on multichannel seismic lines (Sager and Kennicutt, 2000). Intact gas hydrate has been recovered from MC 852/853 at water depths of 1050–1060 m by numerous researchers on several cruises suggesting that the gas hydrates are persistent at the site (Sassen and others, 1999a). Here, gas hydrate occurs within gassy sediments containing biodegraded crude oil, contains C_1–C_5 hydrocarbon gases, and is inferred to be structure II.

The estimated maximum thickness of the GHSZ is about 780 m. Salt is present in the near-surface as evidenced by high chloride concentrations (Ussler and Paull, Chapter 8). Core descriptions indicate relatively high hydrate concentration in shallow sediments with up to 90– 100 volume % saturation in some intervals (Sassen and others, 2001a).

Thick, relatively unfaulted sediments overlie the reservoir section of the Ursa Field. A lack of hydrocarbon seeps directly over Ursa Field suggests that the unfaulted section is relatively impermeable. Part of the sub-regional fluid flow is channeled laterally along sand carrier beds out of the basin to a major fluid flow release point over the shallow salt on MC853 (Sassen and others, 2001a).

West Mississippi Canyon

West Mississippi Canyon is an area with widespread sea floor deformation and shallow structures, and gas hydrate (fig. 5). Cooper and Hart (2003) found irregular and diffuse HRZs above diapiric structures, along high angle fault zones, laterally within layered and chaotic stratal units bounded by fault, and adjacent to acoustic wipe-out zones. Gas is the likely cause of the high reflectivity; thus localized concentrations of upward migrating gas are moving into shallow reservoirs adjacent to faults potentially forming gas hydrate. Gas hydrate was recovered in a core from a diapir west of our study area (Sassen and others, 1994). In other areas of the Gulf of Mexico's upper continental slope where acoustic wipe-out zones and diffuse HRZs are seen, massive deformation, flow units, gas hydrate and diagenetic carbonates are found within the near-sea floor sediments (Roberts, 2001).

Results and Discussion

Sediment gas was extracted from 99 samples from 23 holes and classified according to the origin of the gas in table 2: Microbial (M), Mainly (X) microbial methane with some thermogenic hydrocarbons, and Mainly thermal hydrocarbons with some microbial methane (TX). Sample depths ranged from 90 to 3740 cm below the sea floor. Eight free gas samples were collected and analyzed.

Tunica Mound

Gas concentrations measured on the flank of Tunica Mound (fig. 2) were highest very near the crest of a subsidiary diapir like structure characterized by signs of active fluid flow. Methane concentrations in the 9-hole transect ranged from 24,000 μL /L in core MD02-2535 to 6 μL /L in core MD02-2538 (figs. 6 to 9, table 2). Methane's carbon isotopic composition ranged from –98.30‰ PDB in core MD02-2545 to –61.20‰ in core MD02-2543; thus all values fall within the range expected of microbially-sourced methane. Ethane and higher molecular weight hydrocarbon gas concentrations were low along the transect with the highest concentration found at a depth of about 27 m in core MD02-2535. We interpret the gas near the mound to be from mainly microbial sources with some mixture of microbial and thermal sources (table 2).

Likely input of thermogenic gases are limited to within the mound (not successfully cored due to armoring by carbonate) and very near the mound. In general, we find the isotopic signature of methane to be lighter than expected for the entire study area. Sassen and others, (2003) have speculated about a deep seated source of microbial gas in the northern Gulf of Mexico, and this may be the case here and elsewhere we cored.

Free gas samples were collected from cores MD02-2537 and 2546 (table 3). Gas concentrations have been normalized to methane to eliminate the dilution of atmospheric gases that are considered artifacts of the sampling technique. Gas concentrations of the free gas indicate that it is of microbial origin with greater than 99% methane, less than 0.1% ethane, and up to about 8 ppm propane. The methane is of microbial carbon isotopic composition ranging from –82.2‰ to –72.2‰. The above data and the presence of high chloride concentrations (up to 2,100 mM) and shallow sulfate-methane interface (SMI, 0 to 13.5 mbsf) Ussler and Paull, Chapter 8, are consistent with fluid flow along high angle faults flanking diapers. All indications of active fluid flow are near background levels approximately 4km from the mound. The SMI ranges from 12-15 mbsf here with chloride concentrations very near those of seawater (about 560 mM), and the hydrocarbon gas composition is indicative of strictly a microbial source of methane.

Pigmy Basin

One gas sample was collected and analyzed from Core MD02-2553 (fig. 3), within this basin. The methane concentration was low, 136 μL/L, with a carbon isotopic composition of –45.7‰, and a similar carbon isotopic composition in CO_2 of –23.8‰. These thermogenic $\delta^{13}C$ coupled with a low concentration of methane indicates that the methane pool has likely been oxidized by methanotrophs (fig. 10, table 2). Higher hydrocarbons are at very low concentrations, and it is concluded that Pigmy Basin may be characterized by microbial sources of methane.

Bush Hill

Beginning on the eastern flank of Bush Hill, three cores were taken at 2 km intervals into the adjoining basin (fig. 4). Methane concentrations in the 3-hole transect ranged from 19,800 μL /L in core MD02-2554 to 195 μL /L in core MD02-2555 (figs. 10 and 11, table 2).The carbon isotopic composition of methane ranges –91.1‰ PDB in core MD02-2545 to –72.8‰ in core MD02-2543; thus all values fall within the isotopic range expected of microbially-sourced

methane. The highest concentration of ethane and higher molecular weight hydrocarbon gases were found in core MD02-2554 at a depth of about 3m, elsewhere concentrations were low.

Free gas samples were collected from cores MD02-2554 and MD02-2555 (table 3). Gases from these samples are of microbial origin with greater than 99% methane, and less than 0.05% ethane, and up to about 4 ppm propane. The microbial sourced methane has carbon isotopic composition ranging from –88.3‰ to –84.2‰.

Chloride concentrations are nearly those of seawater, but increase to 583 mM in core MD02-2554 indicating the slight presence of fluid flow associated with salt dissolution. The shallow SMI ranges from about 7.5 to 13.5 mbsf (Ussler and Paull, Chapter 8) indicative of a substantial methane flux (Borowski and others, 1996). We conclude that the hydrocarbon gases here are of microbial origin.

We did not core on Bush Hill itself, where gas hydrate has been previously sampled. Structure II gas hydrate is abundant at Bush Hill (Sassen and others, 2001b) and shows some variation in composition and isotopic properties across the site and from year to year. Vein-filling gas hydrate is typically found at sites with rapid fluid flow (Ginsburg and Soloviev, 1998). It appears that fluid flow bringing thermogenic hydrocarbon gases to the sea floor is confined to a small venting area.

A vent gas sample collected from Bush Hill in 1998 (Sassen and others, 1999) contained thermogenic methane (93.4%), and individual C_2-C_5 hydrocarbons generally decreasing with increasing molecular weight. The $\delta^{13}C$ of this vent methane is -44.9‰ and the δD is -171‰ SMOW. The $\delta^{13}C$ of the CO_2 of the vent gas is +13.2‰, clearly thermogenic. The $\delta^{13}C$ of Bush Hill gas hydrate methane had isotopic values similar to the vent gas with $\delta^{13}C$ and δD of methane at -43.6‰ and -167‰, respectively, and CO_2 $\delta^{13}C$ of +17.5‰. Relative to the vent gases which it likely precipitated from, the gas hydrate-bound gases, methane occurs in lower percentage (72.1%), and the higher molecular weight hydrocarbons occur in higher concentration (Sassen and others, 2001b).

Mississippi Canyon Region

Kane Spur

Methane concentrations in 5 cores ranged from 1,670 μL/L in core MD02-2559 to 6 μL/L in core MD02-2555 (figs. 12,13 and 15, table 2). The $\delta^{13}C$ of methane ranged from

–93.6‰ PDB in core MD02-2560 to –62. 6‰ in core MD02-2561, with all values falling within the isotopic range expected of microbially-sourced methane. Ethane and higher molecular weight hydrocarbon gas concentrations were low in each of the five cores with the highest concentration of ethane found in core MD02-2567 (5.14 μL/L) at a depth of 13.4 m. We conclude that the minor volumes of gas present in the upper 35 m of sediment on Kane Spur are of microbial origin.

Chloride concentrations are those of seawater, between 566 to 579 μM indicative of the lack of fluid flow associated with salt dissolution within the upper 35 meters of sediment. The SMI in this area is deeper than our cores and could not be penetrated. In addition, the sulfate concentrations increase slightly with depth (Ussler et al, this report) indicative of very little methane flux. We conclude that the minor volumes of gas present in the upper 35 m of sediment on Kane Spur are of microbial origin.

MC853

A three hole transect beginning near the MC853 diapir was cored. Core MD02-2566, notable for the lack of hydrocarbon gases was taken on the southeast flank of the diapir. Two cores were taken on the summit of the diapir MD02-2563 and MD02-2565. These cores were noted for the presence of visible oil and gas of clearly thermogenic origin. Both cores contained disseminated gas hydrate, with the majority found in core MD02-2565 as indicated by over-pressuring that resulted in the upper 3-4 m of core exploding out of the core barrel and into the ocean. Vigorous bubbling in the water adjacent to the ship confirmed the presence of gas hydrate (Lorenson and others 2002), although gas hydrate was not preserved or analyzed from this core.

Methane concentrations in the 3-hole transect ranged from 27,300 μL/L in core MD02-2563 to 6 μL/L in core MD02-2566 (figs. 14 and 15, table 2). The $\delta^{13}C$ of methane spans from –52.2‰ in core MD02-2563 to –60.1‰ in core MD02-2565. These values fall within the isotopic range expected of microbially-sourced methane; however, the visible presence of oil and higher molecular weight hydrocarbon gases in the core clearly confirm the presence of thermogenic hydrocarbons. Ethane and higher molecular weight hydrocarbon gas concentrations were higher near and on the diapir, with the highest

ethane concentration of 1,060 μL/L found in core MD02-2565 at a depth of 12 m. The carbon isotopic composition of ethane was –28.8‰, indicative of a thermal origin.

In addition to ethane, higher molecular weight hydrocarbons up to normal pentane were analyzed for $\delta^{13}C$. Typically the carbon isotopic composition of hydrocarbon gas becomes heavier with increasing carbon number; however, isobutane $\delta^{13}C$ is lighter (–28.5‰) than the either propane (–27.6‰) or normal butane (–26.5‰). Typically this result is an indication of either multiple sources, or that some fractionation is occurring between the sediment gas and gas hydrate. Because there is no compelling evidence of multiple thermogenic sources of gas, we believe this is likely due to the isotopic fractionation of isobutane into Structure II gas hydrate. Gas hydrate gas composition from this diapir has been previously described by Sassen and others, (2001). They measured about 75% methane in four samples with a mean $\delta^{13}C$ of –46.6‰ a thermal source of methane and other hydrocarbon gases was suggested. The carbon isotopic composition of higher molecular weight hydrocarbons also showed the same trend described above for sediment gases, thus it is concluded that the sediment gas reflects the composition of gas hydrate here with the notable exception of methane. Methane is preferentially excluded by gas hydrate formation in favor of higher molecular weight hydrocarbons, and is isotopically heavier (Sassen and others, 2001b).

Free gas collected from core MD02-2565 (table 3) is of mixed microbial and thermal origin. Gas measured from this core is composed of 92% methane, 2.5% ethane, 2.3% propane and other higher weight hydrocarbon gases. The carbon isotopic composition of methane is –61.8‰ suggesting a microbial origin and indicating that there is a significant contribution of methane from microbial sources in addition to the obvious presence of thermogenic higher molecular weight hydrocarbons.

Chloride concentrations in core MD02-2566 are nearly those of seawater, indicating little fluid flow, however the chloride concentrations are much higher (up to 2270 μM in core MD02-2565) on the diapir suggesting rapid fluid flow. Sulfate concentrations are higher than seawater values in core MD02-2566 similar to those on Kane Spur (Ussler and Paull, chapter 8). On the diapir, the SMI is shallow and ranges from about 1.5 to 2.5 mbsf (Ussler and Paull, chapter 8) indicative of a substantial methane flux. We conclude that

the hydrocarbon gases here are mainly thermogenic with a component of microbially sourced methane.

West Mississippi Canyon

In this section of the study gas chimneys and shallow faults were observed very near the sea floor by Cooper and Hart (2003), and in the thalweg of Mississippi Canyon on lease block MC802 where gas hydrate had previously been observed (Sassen and others, 1994). Gas hydrate was recovered within MC802 in cores MD02-2569 and 2573, both taken on top of the same sea floor mound, but only in adequate amounts to obtain gas analyses from core MD02-2569. Core MD02-2573 was intended to be for heat flow measurements; however, we recovered a bent-barrel core with visible gas hydrate in the core-catcher. It is assumed the core met refusal at a gas hydrate layer or an authgenic carbonate layer which caused the barrel to bend.

Methane concentrations in the three holes cored in this area ranged 19,900 μL/L in core MD02-2573 to 1410 μL/L in core MD02-2569 (figs. 15 and 16, table 2), The methane $\delta^{13}C$ values ranged from –72.4‰ PDB in core MD02-2570 to –59.5‰ in core MD02-2569, therefore, all values fall within the isotopic range expected of microbially-sourced methane. Ethane and higher molecular weight hydrocarbon gas concentrations were generally low with the highest ethane concentration of 70.7 μL/L found in core MD02-2573 at a depth of 2.6 m.

Three free gas samples were collected from core MD02-2570 at depths of 15, 18, and 20m (table 3). These samples were composed of primarily methane (99%) with smaller amounts of ethane (0.03%) and propane (300 ppm) indicating mainly a microbial origin. A modest amount of thermogenic hydrocarbons were found in the shallowest sample (15 m) while the lower samples have much less, suggesting some vertical heterogeneity or lateral gas migration pathways. The mean $\delta^{13}C$ of methane of –70.3‰ suggests a microbial origin.

Lenticular bodies of gas hydrate were sampled in core MD02-2569 at two depths, 3.8 and 7.0 mbsf. Results of controlled gas hydrate dissociation are given in Table 4. The quality of the gas hydrate recovered was poor due to core recovery time approaching two hours. Low gas to water ratios from dissociated samples with a maximum of 33 (170 for a fully saturated gas hydrate) confirming that the samples had previously decomposed.

The composition of gas hydrate is principally methane, 95.0 to 99.5%, followed by CO_2 concentrations ranging from 0.16% to 4.0%. Higher molecular weight hydrocarbon gases; ethane, propane and isobutane are found in concentrations exceeding 1000 ppm suggesting that both structure I and structure II gas hydrate are present. The lack of normal butane suggests that gas hydrate formation here is from lean thermogenic gas (for example the free gas composition) selectively incorporating isobutane. A similar effect has been noted in Arctic gas hydrate accumulations by Lorenson at al., (1999).

Chloride concentrations are nearly those of seawater in core MD02-2570 indicating little fluid flow associated with diapirism; however, the presence of gas and shallow faults in the seismic records (appendix D, this report) indicate the flow of gas without salt. Chloride concentrations are much higher (865 mM) in core MD02-2569 suggesting fluid flow associated with salt. Unpublished industry 3D seismic records suggest the MD02-2569 site is likely a diapiric structure. The SMI is shallow and ranges from 10.5 to 7.5 mbsf (Ussler and Paull, chapter 8) indicating substantial methane flux. In conclusion, the hydrocarbon gases here are of mainly microbial origin, with a component of thermogenic hydrocarbons at site MD02-2569.

Origin of gases

The majority of hydrocarbon gases encountered in this study are of microbial origin. Sassen and others, (2003) have speculated that there is a deep seated source of microbial gas in the northern Gulf of Mexico and this observation agrees with our data.

Thermogenic gases are present in cores that are on or very near sea floor features that exhibit active fluid venting. These area are typically along the rims of salt withdrawal basins and active diapirism. In the northern Gulf of Mexico this diapirism is commonly associated with saline fluids that limit the extent of the gas hydrate stability field to the near surface. Methane carbon isotopic composition versus the gas wetness ratio C_1/C_2+C_3 for core gas is plotted in figs. 17 and 18. Primary fields representing accepted values for microbial and thermogenic sourced methane gas are noted. Most of the data fall outside these boundaries likely reflecting mixing of microbial methane with thermogenic methane.

Table Captions

Table 1. Location of cores in this study.

Table 2. Composition of hydrocarbon gas and carbon dioxide of core samples.

Table 3. Composition of hydrocarbon gas and carbon dioxide of free gas normalized to methane. Free gas was collected by drilling a hole into the core liner, then inserting a syringe to collect gas.

Table 4. Composition of hydrocarbon gas and carbon dioxide of gas hydrate gas normalized to methane. Gas was collected in syringes after controlled dissociation.

Figure Captions

Figure 1. Index map of locations in this report.

Figure 2. Cores sites adjacent to Tunica Mound. Gravity and giant piston cores noted with yellow and red stars respectively. Other core observations indicated as follows. T = measured geothermal gradient (degrees C/km); Cl = chloride ion concentration (μM) maximum at the corresponding depth (mbsf); and SO_4 = sulfate ion concentration (μM) minimum at the corresponding depth (mbsf) indication the depth to the sulfate-methane interface (SMI).

Figure 3. Cores sites adjacent to Tunica Mound. Gravity and giant piston cores noted with yellow and red stars respectively. Other core observations indicated as follows. T = measured geothermal gradient (degree C/km); Cl = chloride ion concentration (μM) maximum at the corresponding depth (mbsf); and SO_4 = sulfate ion concentration (μM) minimum at the corresponding depth (mbsf) indication the depth to the sulfate-methane interface (SMI) (see Ussler and Paull, chapter 8).

Figure 4. Cores sites adjacent to Bush Hill. Gravity and giant piston cores noted with yellow and red stars respectively. Other core observations indicated as follows. T = measured geothermal gradient (degreeC/km); Cl = chloride ion concentration (μM) maximum at the

corresponding depth (mbsf); and SO_4 = sulfate ion concentration (μM) minimum at the corresponding depth (mbsf) indication the depth to the sulfate-methane interface (SMI).

Figure 5. Cores sites in the Mississippi Canyon region. Contours in meters. Gravity and giant piston cores noted with yellow and red stars respectively. Other core observations indicated as follows. T = measured geothermal gradient (°C/km), nm+ not measured; Cl = chloride ion concentration (μM) maximum at the corresponding depth (mbsf); and SO_4 = sulfate ion concentration (μM) minimum at the corresponding depth (mbsf) indication the depth to the sulfate-methane interface (SMI), up w/depth = SO_4 concentration increases with depth.

Figure 6 Plots of diagnostic sediment gas molecular composition and hydrocarbon ratios for hole MD02-2338 and MD02-2339. Core locations are shown in figure 2.

Figure 7. Plots of diagnostic sediment gas molecular composition and hydrocarbon ratios for hole MD02-2338 and MD02-2339. Core locations are shown in figure 2.

Figure 8 Plots of diagnostic sediment gas molecular composition and hydrocarbon ratios for hole MD02-2341 and MD02-2343. Core locations are shown in figure 2.

Figure 9. Plots of diagnostic sediment gas molecular composition and hydrocarbon ratios for hole MD02-2345 and MD02-2346. Core locations are shown in figure 2.

Figure 10. Plots of diagnostic sediment gas molecular composition and hydrocarbon ratios for hole MD02-2353 and MD02-2354. Core locations are shown in figures 3 and 4.

Figure 11. Plots of diagnostic sediment gas molecular composition and hydrocarbon ratios for hole MD02-2355 and MD02-2356. Core locations are shown in figure 4.

Figure 12. Plots of diagnostic sediment gas molecular composition and hydrocarbon ratios for hole MD02-2359 and MD02-2360. Core locations are shown in figure 5.

Figure 13. Plots of diagnostic sediment gas molecular composition and hydrocarbon ratios for hole MD02-2361 and MD02-2362. Core locations are shown in figure 6.

Figure 14. Plots of diagnostic sediment gas molecular composition and hydrocarbon ratios for hole MD02-2363 and MD02-2365. Core locations are shown in figure 6.

Figure 15. Plots of diagnostic sediment gas molecular composition and hydrocarbon ratios for hole MD02-2366 and MD02-2367, and MD02-2370. Core locations are shown in figure 6.

Figure 16. Plots of diagnostic sediment gas molecular composition and hydrocarbon ratios for hole MD02-2369 and MD02-2373. Core locations are shown in figure 6

Figure 17. Plot of methane carbon isotopic composition versus the gas wetness ratio C1/C2+C3 for Tunica Mound core gas. Primary fields representing accepted values for microbial and thermogenic sourced methane gas are noted. Carbon isotopic compositions less than -90 are not plotted but are noted by core number with relative gas wetness ratios indicated by position on the y-axis.

Figure 18. Plot of methane carbon isotopic composition versus the gas wetness ratio C1/C2+C3 for Kane Spur (59, 60, 61, and 62), MC853 (63 and 65), and West Mississippi Canyon (69, 70, and 73) core gas. Primary fields representing accepted values for microbial and thermogenic sourced methane gas are noted. Carbon isotopic compositions less than -90 are not plotted but are noted by core number with relative gas wetness ratios indicated by position on the y-axis

References

Aharon, P., and Fu, B., 2000, Microbial sulfate reduction rates and sulfur and oxygen isotope fractionations at oil and gas seeps in deepwater Gulf of Mexico: Geochimica et Cosmochimica Acta, v. 64, n. 2, 233-246.

Berryhill, H.L., Suter, J.R., and N.S., Hardin, 1987, Late Quaternary facies and structure, northern Gulf of Mexico: AAPG Studies in Geology, n. 23, 289p.

Borowski, W. S., Paull, C. K., and Ussler, W.,III. 1996, Marine pore-water sulfate profiles indicate in situ methane flux from underlying gas hydrate: Geology, v. 24, n. 7, 655-658.

Coleman, J.M., Prior, D.B., and J.F. Lindsay, 1983, Deltaic influences on shelf edge instability processes: SEPM Special Publication 33, 121-137.

Cooper A.K., and Hart, P.E., 2003, High Resolution seismic-reflection investigation of the northern Gulf of Mexico gas-hydrate-stability zone. Marine and Petroleum Geology: v. 19, 1275-1293.

Cook, D., D'Onfro, P., 1991, Jolliet Field thrust structure and stratigraphy, Green Canyon Block 184, offshore Louisiana: Trans.- Gulf Coast Assoc. Geol. Soc., v. 41, 100– 121.

Eaton, L.F., 1999, Drilling through shallow water flow zones at Ursa: Conference Proceedings Shallow water-flows, Oct. 6-8, 1999, Penn Well, Tulsa, OK, 600 p.

Ginsburg, G.D., and Soloviev, V.A., 1998, Submarine gas hydrates: St. Petersburg, Russia, VNII Okeangeologia, 216 p.

Goodwin, R.H. and D.B. Prior, 1989, Geometry and depositional sequences of the Mississippi Canyon, Gulf of Mexico: Journal of Sedimentary Petrologists, v. 59, n. 2, 318-329.

Kennicutt II, M.C., Brooks, J.M., and Denoux, G.J., 1988, Leakage of deep, reservoired petroleum to the near surface of the Gulf of Mexico continental slope. Marine. Chemistry, v. 24, 39–59.

Kvenvolden, K.A., and Redden G. D., 1980, Hydrocarbon gas in sediment from the shelf, slope, and basin of the Bering Sea. Geochim. Cosmochim. Acta, v. 44, 1145-1150.

Kvenvolden, K.A., Claypool, G.E., Threlkeld, C.N., and Sloan, D.E., 1984, Geochemistry of a naturally occurring massive marine gas hydrate: *In* Schenck, P.A., deLeeuw, J.W., and Lijmbach, G.W.M., (Eds.), Advances in Organic Geochemistry 1983, Org. Geochem., v 6, 703-713.

Lorenson, T.D., Whiticar, M., Waseda, A., Dallimore, S.R., and Collett, T.S., 1999, Gas composition and isotopic geochemistry of cuttings, core, and gas hydrate from the JAPEX/JNOC/GSC Mallik 2L-38 gas hydrate research well: Geological Survey of Canada Bulletin 544, p.143-163.

Lorenson, T.D., Winters, W., Hart, P.E., and Paull, C.K., 2002, Gas Hydrate Occurrence in the Northern Gulf of Mexico Studied with Giant Pistion Cores: EOS, Transactions, American Geophysical Union, v. 83, n. 51 p. 601 and 607.

MacDonald, I.R., Boland, G.S., Baker, J.S., Brooks, J.M., Kennicutt II, M.C., and Bidigare, R.R., 1989, Gulf of Mexico hydrocarbon seep communities: II. Spatial distribution of seep organisms and hydrocarbons at Bush Hill. Marine Biology, v. 101, 235– 247.

MacDonald, I.R., Guinasso Jr., N.L., Sassen, R., Brooks, J.M., Lee, L., and Scott, K.T., 1994, Gas hydrate that breaches the sea floor on the continental slope of the Gulf of Mexico: Geology v. 22, 699–702.

MacDonald, I.R., Reilly Jr., J.F., Best, S.E., Venkataramaiah, R., Sassen, R., Amos, J., and Guinasso Jr., N.L. 1996, A remote-sensing inventory of active oil seeps and chemosynthetic communities in the northern Gulf of Mexico. In: Schumacher, D., Abrams, M.A. (Eds.), Hydrocarbon Migration and its Near-Surface Expression. AAPG Memoir 66, 27– 37.

Minerals Management Service, 2001, Shallow water flows in the northern Gulf of Mexico http://www.gomr.mms.gov/homepg/offshore/safety/wtrflow.html

Roberts, H.H., 2001, Fluid and gas expulsion on the northern Gulf of Mexico continental slope: mud-prone to mineral-prone responses: *in* C.K. Paull and W.P. Dillon, Eds., Natural Gas Hydrate: Occurrence, Distribution, and Dynamics, AGU Monograph Series 24, 145-161.

Roberts, H.H., and R. Carney, 1997, Evidence of episodic fluid, gas and sediment venting on the northern Gulf of Mexico continental slope: Economic Geology, v. 92, 863-879.

Rowan, M.G., and P. Weimer, 1998, Salt-sediment interaction, northern Green Canyon and Ewing Bank (Offshore Louisana), northern Gulf of Mexico: AAPG Bulletin, v.82, 1055-1082.

Sager, W. W., and Kennicutt, M. C. 2000, Proposal for ocean drilling program research on gas hydrate in the Gulf of Mexico: Proceedings Offshore Technology Conference, 1, OTC 12111.

Sassen, R., Roberts, H.H., Aharon, A., Larkin, J., Chinn, E.W., and Carney, R., 1993, Chemosynthetic bacterial mats at cold hydrocarbon seeps. Gulf of Mexico continental slope. Organic Geochemistry, v. 20, 77– 89.

Sassen, R., MacDonald, I.R., Requejo, A.G., Guinasso, N.L., Kennicutt II, M.C., Sweet, S.T. and J.M. Brooks, 1994, Organic geochemistry of sediments from chemosynthetic communities, Gulf of Mexico slope: Geo-Marine Letters, v. 14, 110-119.

Sassen, R., MacDonald, I.R., Guinasso, N.L., Joye, S., Requejo, A.G., Sweet, S.T., Alcala-Herrera, J., DeFreitas, D.A., Schink, D.R., 1998, Bacterial methane oxidation in

sea-floor gas hydrate. Significance to life in extreme environments: Geology v. 26, 289–293.

Sassen, R., Sweet, S.T., Milkov, A.V., DeFreitas, D.A., Salata, G.G., McDade, E.C., 1999a, Geology and geochemistry of gas hydrates, central Gulf of Mexico continental slope: Trans. Gulf Coast Assoc. Geol. Soc. v. 49, 462–468.

Sassen, R, Joye, S., Sweet, S.T., DeFreitas, D.A., Milkov, A.V., and I.R. MacDonald, 1999b, Thermogenic gas hydrates and hydrocarbon gases in complex chemosynthetic communities, Gulf of Mexico continental slope: Organic Geochemistry, v. 30, 485-497.

Sassen, R., Losh, S.L., Cathles III, L., Roberts, H.H., Whelan, J.K., Milkov, A.V., Sweet, S.T., and DeFreitas, D.A., 2001a, Massive vein-filling gas hydrate: relation to ongoing gas migration from the deep subsurface of the Gulf of Mexico. Marine and Petroleum Geology, 18, 551–560.

Sassen, R., Sweet, S.T., Milkov, A.V., DeFreitas, D.A., and Kennicutt II, M.C., 2001b, Thermogenic vent gas and gas hydrate in the Gulf of Mexico slope: Is gas hydrate decomposition significant. Geology v. 29, 107–110.

Sassen, R., Sweet, S.T., Milkov, A.V., DeFreitas, D.A., and Kennicutt II, M.C., 2001c, Stability of thermogenic gas hydrate in the Gulf of Mexico: constraints on models of climate change. In: Paull, C.K., Dillon,W.P. (Eds.), Natural Gas Hydrates: Occurrence, Distribution, and Detection. American Geophysical Union, Washington, DC, 131– 143.

Sassen, R., Milkov, A. V., Ozgul, E., Roberts, H. H., Hunt, J. L., Beeunas, M. A., and others, 2003, Gas venting and subsurface charge in the Green Canyon area, Gulf of Mexico continental slope; evidence of a deep bacterial methane source?: Organic Geochemistry, v. 34, 10, 1455-1464.

Weimer, P., Crews, J.R., Crow, R.S., and P. Varnai, 1998, Atlas of petroleum fields and discoveries, northern Green Canyon, Ewing Bank, and Southern Ship Shoal northern Gulf of Mexico: AAPG Bulletin, v. 82, 878-917.

Core ID	Latitude	Longitude	Area Name
MD02-2535	27.61983	92.24100	Tunica Mound
MD02-2537	27.61600	92.24867	Tunica Mound
MD02-2538GHF	27.61667	92.24717	Tunica Mound
MD02-2539	27.63967	92.19217	Tunica Mound
MD02-2541	27.63250	92.21233	Tunica Mound
MD02-2542GHF	27.63217	92.21200	Tunica Mound
MD02-2543G	27.61233	92.25550	Tunica Mound
MD02-2545G	27.61400	92.25167	Tunica Mound
MD02-2546	27.61567	92.24700	Tunica Mound
MD02-2548	27.63750	92.19950	Tunica Mound
MD02-2553C2	27.18350	91.41667	Pigmy Basin
MD02-2554	27.78333	91.49900	Bush Hill Basin
MD02-2555	27.78317	91.48917	Bush Hill Basin
MD02-2556	27.78300	91.47750	Bush Hill Basin
MD02-2559	28.22250	89.08817	Kane Spur
MD02-2560	28.24333	89.15500	Kane Spur
MD02-2561	28.20517	89.02017	Kane Spur
MD02-2562	28.07983	89.14017	Kane Spur
MD02-2563	28.12333	89.13633	Kane Spur
MD02-2565	28.12350	89.13950	Kane Spur
MD02-2566	28.11917	89.10317	Kane Spur
MD02-2567	28.10017	89.01983	Kane Spur
MD02-2569	28.15217	89.47967	West Mississippi
MD02-2570	29.57100	89.68983	West Mississippi
MD02-2572GHF	28.07100	89.68967	West Mississippi
MD02-2573GHF	28.15200	89.47983	West Mississippi

G= Gravity Core
GHF= Gravity Heat Flow Core
C2= Box Core

Table 1. Locations of cores measured for gas composition.

Table 2. Composition of hydrocarbon gas and carbon dioxide of core samples.

Core	Depth (cm)	CO_2 µL/L	C_1 µL/L	C_2 µL/L	C_3 µL/L	iC_4 µL/L	nC_4 µL/L	neo-C_5 µL/L	iC_5 µL/L	n-C_5 µL/L	c C_5 µL/L
2535	440	435	49	0.16	0.17	0.14	0.10	0.00	0.09	0.11	0.00
2535	590	1404	166	0.40	0.61	0.53	0.25	0.00	0.20	0.06	0.24
2535	1190	774	33	0.09	0.02	0.00	0.00	0.00	0.00	0.18	0.00
2535	2390	1115	23847	6.97	3.07	1.33	0.27	4.43	0.36	0.06	0.30
2535	2690	1004	17240	80.57	31.19	9.32	1.31	42.04	1.23	0.00	0.00
2535	2840	1191	17750	0.33	0.43	0.16	0.18	0.04	0.10	0.06	0.16
2537	440	144	938	0.80	0.41	0.23	0.17	0.02	0.13	0.06	0.26
2537	890	337	748	3.20	0.34	0.02	0.05	0.00	0.01	0.00	0.00
2537	1640	205	2242	4.56	0.57	0.14	0.19	0.11	0.29	0.08	0.31
2537	2090	350	4587	5.29	0.57	0.18	0.22	0.02	0.11	0.05	0.14
2537	3240	209	7089	9.49	0.96	0.34	0.33	0.03	0.40	0.09	0.34
2538	140	96	6	0.39	0.07	0.00	0.01	0.02	0.01	0.00	0.00
2538	290	145	7	0.43	0.07	0.06	0.06	0.07	0.17	0.07	0.21
2538	440	94	174	0.51	0.75	0.71	0.50	0.02	0.40	0.16	0.62
2538	590	390	1353	3.73	0.24	0.01	0.04	0.02	0.01	0.01	0.00
2538	740	382	1231	2.19	0.21	0.02	0.06	0.02	0.02	0.00	0.00
2539	140	75	11	0.24	0.04	0.00	0.00	0.00	0.00	0.00	0.00
2539	890	1221	19	0.36	0.08	0.00	0.02	0.01	0.00	0.00	0.00
2539	1640	1130	10105	0.03	0.30	0.02	0.05	0.01	0.00	0.00	0.00
2539	2390	431	7233	0.10	0.18	0.17	0.12	0.13	0.34	0.11	0.43
2539	2990	381	5434	0.11	0.07	0.00	0.02	0.01	0.01	0.00	0.00
2541	130	56	20	0.24	0.03	0.01	0.00	0.02	0.04	0.00	0.05
2541	740	1027	10	0.25	0.04	0.00	0.01	0.01	0.00	0.00	0.00
2541	1490	504	2637	0.00	0.06	0.00	0.02	0.01	0.01	0.00	0.00
2541	2240	298	6107	0.01	0.13	0.03	0.05	0.04	0.09	0.04	0.11
2543	900	266	16881	27.60	15.15	8.82	1.39	3.49	2.40	0.11	0.20
2545	200	419	14481	8.19	0.40	0.02	0.06	0.03	0.01	0.01	0.00
2545	390	109	10943	7.81	1.39	0.18	0.27	0.04	0.04	0.01	0.00
2545	500	77	9581	9.07	1.49	0.17	0.30	0.06	0.05	0.01	0.00
2545	690	1072	7444	11.45	1.76	0.23	0.34	0.14	0.23	0.05	0.21
2545	890	186	10353	6.28	1.22	0.12	0.27	0.18	0.07	0.02	0.00

2546	140	167	404	0.52	0.02	0.01	0.01	0.01	0.03	0.01	0.02
2546	740	124	551	0.90	0.12	0.07	0.06	0.06	0.17	0.04	0.17
2546	1340	291	2277	4.92	0.27	0.05	0.07	0.00	0.02	0.01	0.00
2546	1790	220	9625	14.07	0.63	0.29	0.29	0.11	0.27	0.08	0.25
2546	2240	107	11391	8.01	0.30	0.07	0.12	0.02	0.04	0.02	0.00
2546	2990	131	9308	12.65	1.27	0.21	0.26	0.07	0.14	0.04	0.00
2553	2814	1246	136	0.72	0.10	0.04	0.04	0.01	0.03	0.10	0.03
2554	140	556	1386	0.53	0.29	0.16	0.34	0.05	0.20	0.18	0.10
2554	300	1241	9399	29.09	2.88	0.12	0.24	0.02	0.05	0.00	0.00
2554	600	309	19750	8.70	2.10	0.02	0.10	0.03	0.02	0.02	0.00
2554	2065	1437	7574	12.39	1.98	0.39	1.21	0.05	0.91	0.47	0.20
2554	2665	1061	10081	19.30	1.89	0.08	0.19	0.02	0.04	0.02	0.00
2555	600	177	5148	3.42	0.17	0.02	0.08	0.04	0.01	0.01	0.00
2555	740	1353	195	0.27	0.10	0.01	0.03	0.03	0.01	0.01	0.00
2555	2240	556	3690	0.35	0.34	0.02	0.09	0.01	0.01	0.01	0.00
2556	1490	923	7476	3.42	0.81	0.39	0.89	2.74	0.67	0.28	0.15
2556	2090	2143	11283	2.05	7.99	1.78	9.45	0.06	5.04	2.51	0.62
2556	2990	894	3818	0.40	0.72	0.12	0.35	0.03	0.16	0.00	0.10
2556	3740	1587	3535	0.38	0.80	0.13	0.23	0.03	0.07	0.00	0.07
2559	740	3043	6	0.39	0.09	0.00	0.03	0.05	0.01	0.80	0.00
2559	1450	1660	21	0.82	0.55	0.46	0.42	0.03	0.39	0.21	0.00
2559	2090	977	1673	0.64	0.16	0.18	0.10	0.00	0.07	0.05	0.12
2559	2840	1681	37	1.26	0.27	0.14	0.36	0.03	0.33	0.12	0.08
2559	3290	948	21	1.03	0.18	0.06	0.14	0.02	0.12	0.05	0.03
2560	140	158	38	0.29	0.14	0.07	0.07	0.03	0.08	0.03	0.07
2560	730	4742	944	0.47	0.27	0.23	0.10	0.00	0.06	0.03	0.00
2560	1490	2611	8	0.87	0.10	0.02	0.02	0.03	0.02	0.05	0.00
2560	2090	1543	150	0.92	0.16	0.08	0.08	0.02	0.09	0.03	0.08
2561	590	525	68	0.47	0.12	0.03	0.03	0.00	0.01	0.03	0.00
2561	1180	2555	166	0.99	0.67	0.33	0.70	0.49	0.35	0.30	0.16
2561	1790	1017	9	0.87	0.21	0.13	0.26	0.02	0.11	0.02	0.05
2561	2390	2067	393	1.37	0.64	0.56	0.37	0.02	0.29	0.10	0.00
2561	2840	1311	22	0.89	0.73	0.26	0.89	0.04	0.75	0.37	0.16
2562	440	1959	17	0.15	0.15	0.11	0.08	0.00	0.06	0.00	0.09
2562	730	11387	7	0.71	0.23	0.09	0.20	0.05	0.21	0.09	0.07

2562	890	2596	147	0.51	0.38	0.29	0.22	0.02	0.14	0.05	0.18
2562	1490	1280	9	0.59	0.13	0.08	0.11	0.02	0.11	0.05	0.06
2562	2090	1376	15	0.44	0.13	0.11	0.07	0.01	0.05	0.01	0.06
2562	2450	3082	37	2.21	3.25	1.42	5.52	0.02	2.76	3.54	0.00
2563	90	2695	1976	104.48	13.65	2.37	4.14	11.65	3.63	1.92	0.27
2563	295	5530	22293	393.82	56.87	21.15	7.58	164.83	5.24	0.79	0.05
2563	380	6460	27274	858.40	247.02	107.69	10.41	409.68	13.17	0.62	4.35
2565	440	653	8719	615.00	2322.47	1995.15	655.05	22.44	413.87	87.31	227.44
2565	890	651	13464	710.72	914.68	281.99	1359.92	3.74	1041.04	245.11	26.80
2565	1190	708	16191	1057.77	2038.86	602.47	1150.62	8.41	445.62	238.69	54.40
2565	1640	595	12137	633.55	1175.73	383.08	1066.64	3.70	417.06	254.99	30.38
2565	2240	501	22370	773.56	1006.22	28.86	62.15	1.78	196.04	153.67	29.53
2566	440	702	6	0.27	0.30	0.27	0.14	0.01	0.12	0.09	0.20
2566	890	1300	6	0.35	0.18	0.08	0.18	0.02	0.09	0.12	0.04
2566	1340	2481	12	0.42	0.19	0.16	0.10	0.01	0.08	0.06	0.12
2566	1940	898	8	0.58	0.21	0.08	0.24	0.00	0.11	0.02	0.05
2566	2390	1702	23	1.13	0.16	0.08	0.16	0.03	0.10	0.03	0.06
2567	590	1413	12	0.55	0.17	0.17	0.11	0.01	0.09	0.05	0.15
2567	1340	1297	55	5.14	12.77	5.18	18.34	0.04	8.09	8.69	0.00
2567	1490	2766	44	0.84	0.18	0.13	0.16	0.00	0.10	0.02	0.06
2567	1790	2208	25	1.70	2.33	0.79	3.73	0.02	1.85	2.36	0.50
2567	2090	1535	16	0.58	0.15	0.09	0.09	0.02	0.12	0.01	0.09
2569	995	504	2589	8.14	5.90	10.48	0.05	4.19	0.74	0.13	0.00
2569	1400	89	1412	1.77	3.01	0.91	4.84	0.10	3.27	2.02	0.24
2569	1640	1029	2692	3.16	1.34	0.33	0.43	0.76	0.16	0.12	0.00
2569	2090	997	17223	12.31	3.21	0.41	1.31	0.48	0.91	0.50	0.19
2569	2690	347	4191	65.10	129.30	34.71	114.95	1.16	37.60	19.77	2.07
2570	440	1177	3507	2.67	1.02	0.50	0.50	0.05	0.30	0.14	0.00
2570	1040	447	7441	3.27	1.26	0.39	0.63	0.08	0.27	0.38	0.00
2570	1490	1056	4197	6.89	9.94	3.01	6.75	0.36	5.01	1.90	0.55
2570	1790	660	1727	1.63	0.85	0.11	0.13	0.38	0.07	0.10	0.00
2570	2240	295	3116	4.38	2.12	0.56	0.90	0.33	0.72	0.30	0.15
2573	260	611	19870	70.66	5.37	2.56	1.37	55.16	2.21	0.55	0.17

Table 2 continued

Core	Depth (cm)	2,2MC$_4$ µL/L	2MC$_5$ µL/L	3MC$_5$ µL/L	n-C$_6$ µL/L	McC$_5$ µL/L	n-C$_7$ µL/L	McC$_6$ µL/L	C$_1$/C$_2$+C$_3$	iC$_4$/nC$_4$	iC$_5$/nC$_5$
2535	440	0.00	0.01	0.05	0.16	0.00	0.15	0.50	150	1.33	0.83
2535	590	0.01	0.03	0.08	0.20	0.05	0.36	0.46	164	2.10	3.54
2535	1190	0.00	0.02	0.00	0.00	0.00	0.00	0.00	292		
2535	2390	0.75	1.15	0.29	0.46	0.37	0.09	0.30	2376	4.90	5.94
2535	2690	5.03	6.50	0.49	0.42	2.49	0.00	0.00	154	7.11	
2535	2840	0.00	0.04	0.08	0.20	0.00	0.45	0.49	23318	0.89	1.61
2537	440	0.00	0.02	0.09	0.32	0.04	0.41	0.49	775	1.37	2.17
2537	890	0.00	0.00	0.00	0.00	0.00	0.00	0.00	211	0.39	
2537	1640	0.03	0.19	0.41	0.00	1.03	0.84	1.17	436	0.76	3.69
2537	2090	0.00	0.01	0.05	0.12	0.00	0.15	0.28	783	0.84	2.06
2537	3240	0.00	0.10	0.46	0.50	0.86	0.58	0.87	678	1.01	4.48
2538	140	0.00	0.00	0.00	0.00	0.00	0.00	0.00	12	0.00	
2538	290	0.02	0.08	0.21	0.33	0.77	0.82	1.10	14	0.94	2.36
2538	440	0.05	0.06	0.17	0.42	0.12	0.73	0.98	139	1.44	2.54
2538	590	0.00	0.00	0.09	0.22	0.00	0.00	0.00	341	0.30	1.50
2538	740	0.00	0.00	0.00	0.00	0.00	0.00	0.00	513	0.37	
2539	140	0.00	0.00	0.00	0.08	0.00	0.00	0.00	40		
2539	890	0.00	0.00	0.00	0.07	0.00	0.00	0.00	42	0.00	
2539	1640	0.00	0.00	0.00	0.07	0.00	0.00	0.00	30118	0.39	
2539	2390	0.06	0.08	0.30	0.00	1.25	0.94	1.60	26064	1.35	3.10
2539	2990	0.00	0.00	0.00	0.04	0.00	0.00	0.00	30561	0.00	
2541	130	0.00	0.00	0.06	0.11	0.21	0.22	0.25	72		
2541	740	0.00	0.00	0.00	0.03	0.00	0.00	0.00	35	0.00	0.00
2541	1490	0.00	0.00	0.00	0.00	0.44	0.00	0.00	46354	0.00	1.57
2541	2240	0.00	0.03	0.12	0.23	0.44	0.49	0.52	41208	0.54	2.32
2543	900	1.64	5.84	1.81	0.18	0.62	1.03	0.38	395	6.34	21.42
2545	200	0.00	0.00	0.00	0.10	0.00	0.00	0.00	1686	0.33	0.95
2545	390	0.00	0.00	0.00	0.06	0.00	0.00	0.00	1190	0.66	4.12
2545	500	0.00	0.00	0.02	0.05	0.00	0.00	0.00	908	0.56	6.33
2545	690	0.03	0.08	0.24	0.31	0.64	0.60	0.75	564	0.67	4.71
2545	890	0.00	0.02	0.06	0.14	0.00	0.00	0.00	1379	0.44	3.55
2546	140	0.00	0.00	0.00	0.30	0.16	0.19	0.14	747	0.40	2.81

2546	740	0.02	0.08	0.19	0.26	0.47	0.53	0.73	542	1.10	4.63
2546	1340	0.00	0.02	0.00	0.03	0.00	0.00	0.00	438	0.73	2.57
2546	1790	0.04	0.13	0.48	0.50	0.77	0.70	0.87	655	0.98	3.31
2546	2240	0.01	0.00	0.00	0.12	0.00	0.00	0.00	1371	0.64	1.72
2546	2990	0.04	0.05	0.00	0.04	0.00	0.03	0.00	669	0.81	3.27
2553	2814	0.00	0.00	0.02	0.14	0.00	0.08	0.05	166	0.97	0.26
2554	140	0.02	0.01	0.17	0.44	0.10	0.44	0.72	1680	0.48	1.11
2554	300	0.00	0.00	0.04	0.21	0.00	0.00	0.00	294	0.50	
2554	600	0.00	0.00	0.11	0.50	0.00	0.00	0.00	1828	0.16	0.95
2554	2065	0.07	0.22	0.57	0.70	0.75	0.95	0.98	527	0.33	1.94
2554	2665	0.00	0.01	0.05	0.15	0.00	0.00	0.00	476	0.39	1.94
2555	600	0.00	0.00	0.05	0.32	0.00	0.00	0.00	1434	0.20	1.19
2555	740	0.00	0.00	0.04	0.21	0.00	0.00	0.00	528	0.24	0.62
2555	2240	0.00	0.00	0.05	0.15	0.00	0.00	0.00	5339	0.23	1.19
2556	1490	0.17	0.26	0.42	0.47	0.45	0.31	0.49	1769	0.44	2.39
2556	2090	0.44	1.72	2.74	4.33	0.72	5.36	7.88	1123	0.19	2.01
2556	2990	0.01	0.03	0.07	0.22	0.04	0.36	0.52	3410	0.35	
2556	3740	0.00	0.00	0.09	0.27	0.28	0.10	0.23	3008	0.54	
2559	740	0.00	0.00	0.00	0.00	0.00	0.00	0.00	12	0.00	0.02
2559	1450	0.05	0.07	0.18	0.29	0.12	0.50	0.61	16	1.10	1.88
2559	2090	0.00	0.01	0.06	0.15	0.00	0.28	0.47	2081	1.76	1.43
2559	2840	0.01	0.06	0.20	0.36	0.31	0.26	0.30	24	0.38	2.85
2559	3290	0.00	0.02	0.12	0.22	0.14	0.11	0.14	18	0.44	2.50
2560	140	0.00	0.02	0.12	0.24	0.21	0.16	0.24	89	1.08	2.42
2560	730	0.00	0.00	0.02	0.08	0.00	0.18	0.11	1281	2.22	1.92
2560	1490	0.00	0.00	0.00	0.11	0.00	0.00	0.00	9	0.68	0.40
2560	2090	0.00	0.03	0.12	0.20	0.23	0.13	0.22	139	0.99	2.72
2561	590	0.00	0.00	0.00	0.08	0.00	0.00	0.00	116	0.81	0.44
2561	1180	0.06	0.05	0.11	0.38	0.55	0.83	0.81	100	0.47	1.16
2561	1790	0.00	0.01	0.03	0.12	0.01	0.18	0.29	9	0.52	5.67
2561	2390	0.02	0.03	0.13	0.32	0.08	0.40	0.61	196	1.50	2.94
2561	2840	0.04	0.19	0.71	0.59	0.62	0.78	0.93	13	0.29	2.00
2562	440	0.00	0.01	0.04	0.11	0.00	0.20	0.35	56	1.37	
2562	730	0.00	0.06	0.23	0.39	0.32	0.25	0.43	7	0.44	2.42
2562	890	0.00	0.05	0.11	0.28	0.05	0.50	0.82	165	1.32	2.51

2562	1490	0.00	0.02	0.11	0.00	0.20	0.23	0.24	12	0.66	2.20
2562	2090	0.00	0.01	0.03	0.00	0.02	0.16	0.30	26	1.57	5.50
2562	2450	0.16	1.22	1.11	2.91	0.28	1.87	1.31	7	0.26	0.78
2563	90	0.77	1.25	1.93	2.19	1.62	3.79	2.75	17	0.57	1.90
2563	295	9.00	4.88	0.52	0.46	0.33	0.00	0.25	49	2.79	6.64
2563	380	35.11	71.64	5.46	2.77	1.92	0.00	1.20	25	10.34	21.16
2565	440	44.02	95.65	113.69	104.27	39.05	97.70	83.87	3	3.05	4.74
2565	890	58.43	143.10	285.10	159.20	133.63	181.45	151.53	8	0.21	4.25
2565	1190	35.53	116.88	109.62	108.42	24.83	87.76	88.52	5	0.52	1.87
2565	1640	27.65	119.26	106.27	122.31	25.16	112.58	67.31	7	0.36	1.64
2565	2240	6.28	28.60	26.23	32.55	2.95	14.61	8.53	13	0.46	1.28
2566	440	0.01	0.02	0.06	0.19	0.02	0.31	0.38	10	1.84	1.28
2566	890	0.00	0.01	0.04	0.19	0.00	0.11	0.18	11	0.45	0.69
2566	1340	0.00	0.01	0.05	0.16	0.02	0.29	0.48	20	1.51	1.43
2566	1940	0.00	0.01	0.03	0.13	0.01	0.19	0.24	10	0.32	7.07
2566	2390	0.00	0.01	0.05	0.24	0.02	0.20	0.49	18	0.50	3.88
2567	590	0.00	0.01	0.06	0.18	0.03	0.33	0.58	17	1.54	1.73
2567	1340	0.43	2.70	2.28	5.13	0.35	2.33	2.06	3	0.28	0.93
2567	1490	0.00	0.03	0.07	0.19	0.00	0.28	0.47	43	0.82	5.00
2567	1790	0.11	0.90	0.76	2.15	0.23	1.63	1.02	6	0.21	0.78
2567	2090	0.00	0.03	0.16	0.26	0.26	0.16	0.29	22	1.04	9.50
2569	995	0.17	0.89	0.02	8.03	8.01	0.37	0.00	184	201.08	5.77
2569	1400	0.13	0.74	2.49	1.79	1.00	1.37	1.43	296	0.19	1.62
2569	1640	0.00	0.00	0.00	0.18	0.00	0.00	0.00	597	0.77	1.31
2569	2090	0.04	0.23	0.82	0.72	0.63	0.75	0.76	1110	0.31	1.82
2569	2690	2.39	10.46	9.95	10.81	2.32	10.86	7.32	22	0.30	1.90
2570	440	0.02	0.05	0.16	0.32	0.07	0.56	0.71	950	1.02	2.14
2570	1040	0.00	0.10	0.07	0.12	0.00	0.41	0.45	1644	0.61	0.70
2570	1490	0.27	0.76	1.85	1.45	1.56	1.79	2.25	249	0.45	2.64
2570	1790	0.00	0.00	0.00	0.11	0.00	0.33	0.00	695	0.86	0.72
2570	2240	0.04	0.16	0.64	0.66	0.57	0.74	1.01	479	0.62	2.41
2573	260	2.90	1.94	0.37	0.84	0.89	0.00	0.45	261	1.87	3.99

Table 2 continued

Core	Depth (cm)	C_1 $\delta^{13}C$	CO_2 $\delta^{13}C$	C_2 $\delta^{13}C$	C_3 $\delta^{13}C$	i-C_4 $\delta^{13}C$	n-C_4 $\delta^{13}C$	C_5 $\delta^{13}C$	Source
2535	440								M
2535	590	-94.62	-26.52						M
2535	1190								M
2535	2390								M
2535	2690	-93.11	-21.87						X
2535	2840								M
2537	440								M
2537	890								M
2537	1640	-66.00	-18.00						M
2537	2090								M
2537	3240	-74.30	-20.11						M
2538	140								M
2538	290								M
2538	440	-74.50	-45.40						M
2538	590	-71.00	-34.40						M
2538	740	-81.70	-19.70						M
2539	140								M
2539	890								M
2539	1640	-96.60	-33.10						M
2539	2390								M
2539	2990								M
2541	130								M
2541	740								M
2541	1490	-97.10	-26.70						M
2541	2240								M
2543	900	-61.20	-3.00						X
2545	200	-98.30	-43.40						X
2545	390								X
2545	500								X
2545	690	-62.60	-15.20						X
2545	890								X

2546	140	-81.90	-21.20	M
2546	740			M
2546	1340	-75.60	-27.90	X
2546	1790			X
2546	2240			X
2546	2990	-70.80	-11.70	X
2553	2814	-45.67	-23.81	M
2554	140	-83.24	-29.22	M
2554	300	-75.00	-10.40	X
2554	600	-91.10	-43.40	X
2554	2065			X
2554	2665			X
2555	600			X
2555	740			M
2555	2240			M
2556	1490	-85.89	-24.38	X
2556	2090	-72.82	-20.19	X
2556	2990	-84.08	-20.78	M
2556	3740	-81.01	-14.22	M
2559	740			M
2559	1450			M
2559	2090	-64.09	-15.94	M
2559	2840			M
2559	3290			M
2560	140			M
2560	730	-93.59	-20.88	M
2560	1490			M
2560	2090	-72.00	-18.57	M
2561	590			M
2561	1180			M
2561	1790			M
2561	2390	-62.56	-22.51	M
2561	2840			M

2562	440								M
2562	730								M
2562	890	-72.12	-20.61						M
2562	1490								M
2562	2090								M
2562	2450								M
2563	90								TX
2563	295	-53.11	-12.07	-28.15					TX
2563	380	-52.22	-2.23	-28.18	-18.53				TX
2565	440								TX
2565	890								TX
2565	1190	-60.10	-11.10	-28.83	-26.40	-28.44	-25.94	-26.01	TX
2565	1640	-58.87	-3.93	-29.48	-27.63	-28.55	-26.45	-26.51	TX
2565	2240	-59.88	-11.15	-28.96	-26.18		-25.49		TX
2566	440								M
2566	890								M
2566	1340								M
2566	1940								M
2566	2390								M
2567	590								M
2567	1340								M
2567	1490								M
2567	1790								M
2567	2090								M
2569	995	-59.52	-2.71						X
2569	1400	-70.52	-21.33						X
2569	1640	-67.02	-11.40						X
2569	2090	-67.81	-11.55						X
2569	2690	-62.02	-42.48						X
2570	440	-72.35	-28.58						X
2570	1040	-68.74	-13.98						X
2570	1490	-67.14	-11.76						X
2570	1790	-66.55	-10.85						M
2570	2240	-66.38	-14.03						X

2573	260	-62.11	-18.66	-30.08	X

M=Miicrobial
X=Mainly microbial methane with some thermogenic hydrocarbons
TX=Mainly thermal hydrocarbons with some microbial methane

Sample ID core/ depth cm	CO_2	C_1	C_2	C_3	iC_4	nC_4	neo-C_5	iC_5	n-C_5	c C_5	2,2M C_4	$2MC_5$	$3MC_5$	n-C_6	McC_5	n-C_7	McC_6
	ppm																
2537	6261	993343	360.93	7.75	0.63	0.74	3.01	0.04	0.06	0.00	0.00	0.68	6.28	15.22	0.99	0.00	0.00
2546 1600	2259	997076	591.85	2.33	0.64	0.64	5.02	0.00	0.00	0.02	0.00	2.24	20.67	39.29	2.86	0.00	0.00
2554 1642	8326	991287	352.42	4.08	0.11	0.17	2.31	0.00	0.04	0.01	0.00	1.11	8.85	16.99	1.17	0.12	0.00
2555 423	6314	993620	16.42	2.45	0.21	0.44	3.87	0.00	0.04	0.01	0.00	1.57	13.59	25.33	2.04	0.00	0.00
2565	24872	919972	24646	23540	3508.43	2524.31	31.68	560.12	123.51	37.96	16.89	34.69	54.66	37.89	20.29	14.20	4.58
2570 1500	7072	992217	290.34	292.62	61.86	45.38	2.96	10.68	2.43	0.43	0.25	0.66	2.11	1.21	0.46	0.21	0.00
2570 1800	5074	994809	84.64	6.31	0.55	0.48	1.69	0.12	0.06	0.00	0.00	0.53	5.90	14.81	1.37	0.53	0.00
2570 2000	6099	993769	85.89	6.01	0.44	0.00	2.96	0.00	0.00	0.00	0.00	1.97	14.11	20.17	1.10	0.15	0.00

Sample ID core/ depth cm	C_1/C_2+C_3	iC_4/nC_4	iC_5/nC_5	C_1 $\delta^{13}C$	CO_2 $\delta^{13}C$	C_2 $\delta^{13}C$	C_3 $\delta^{13}C$
2537	2694	0.85	0.66	-82.19			
2546 1600	1678	1.00		-72.24			
2554 1642	2781	0.62	0.00	-84.24			
2555 423	52672	0.48	0.00	-88.27			
2565	19	1.39	4.53	-61.83	-13.54	-29.79	-26.5
2570 1500	1702	1.36	4.40	-70.11			
2570 1800	10938	1.14	2.13	-70.61			
2570 2000	10813			-70.28			

Table 3. Composition of hydrocarbon gas and carbon dioxide of free gas normalized to methane. Free gas was collected by drilling a hole into the core liner, then inserting a syringe to collect gas.

Sample	CO_2	C_1	C_2	C_3	iC_4	nC_4	neo-C_5	iC_5	n-C_5	c C_5	2,2MC_4	2MC_5	3MC_5	n-C_6	McC_5	n-C_7	McC_6
	ppm																
2569 380 cm Vial 2	2700	994890	1843.87	460.30	43.50	0.00	29.22	14.42	1.77	0.00	3.02	9.10	1.22	3.88	0.00	0.40	0.00
2569 380 cm Vial 3	40202	949767	7590.37	1079.97	1084.72	6.42	107.47	29.03	0.00	0.00	7.33	26.31	19.37	70.47	0.00	9.64	0.00
2569 380 cm Vial 4	1570	992052	1861.08	2175.54	2245.43	0.00	56.40	16.40	0.00	0.00	3.42	12.51	1.85	4.27	0.00	1.74	0.00
2569 700 cm Vial 3	11407	980376	4093.25	1757.19	2208.34	0.00	61.42	12.27	0.00	0.00	2.75	10.09	8.87	51.85	0.00	11.26	0.00

Sample	Gas to water ratio ml gas/ml water	C_1/C_2+C_3	iC_4/nC_4	C_1 $\delta^{13}C$	CO_2 $\delta^{13}C$
2569 380 cm Vial 2	6.56	432	>1000	-63.26	
2569 380 cm Vial 3	6.56	110	169	-62.12	-14.99
2569 380 cm Vial 4	6.56	246	>1000	-63.11	
2569 700 cm Vial 3	33.14	168	>1000	-54.62	

Gas concentrations normalized to methane
Hydrogen and Helium not measured

Table 4. Composition of hydrocarbon gas and carbon dioxide of gas hydrate gas normalized to methane. Gas was collected in syringes after controlled dissoiciation.

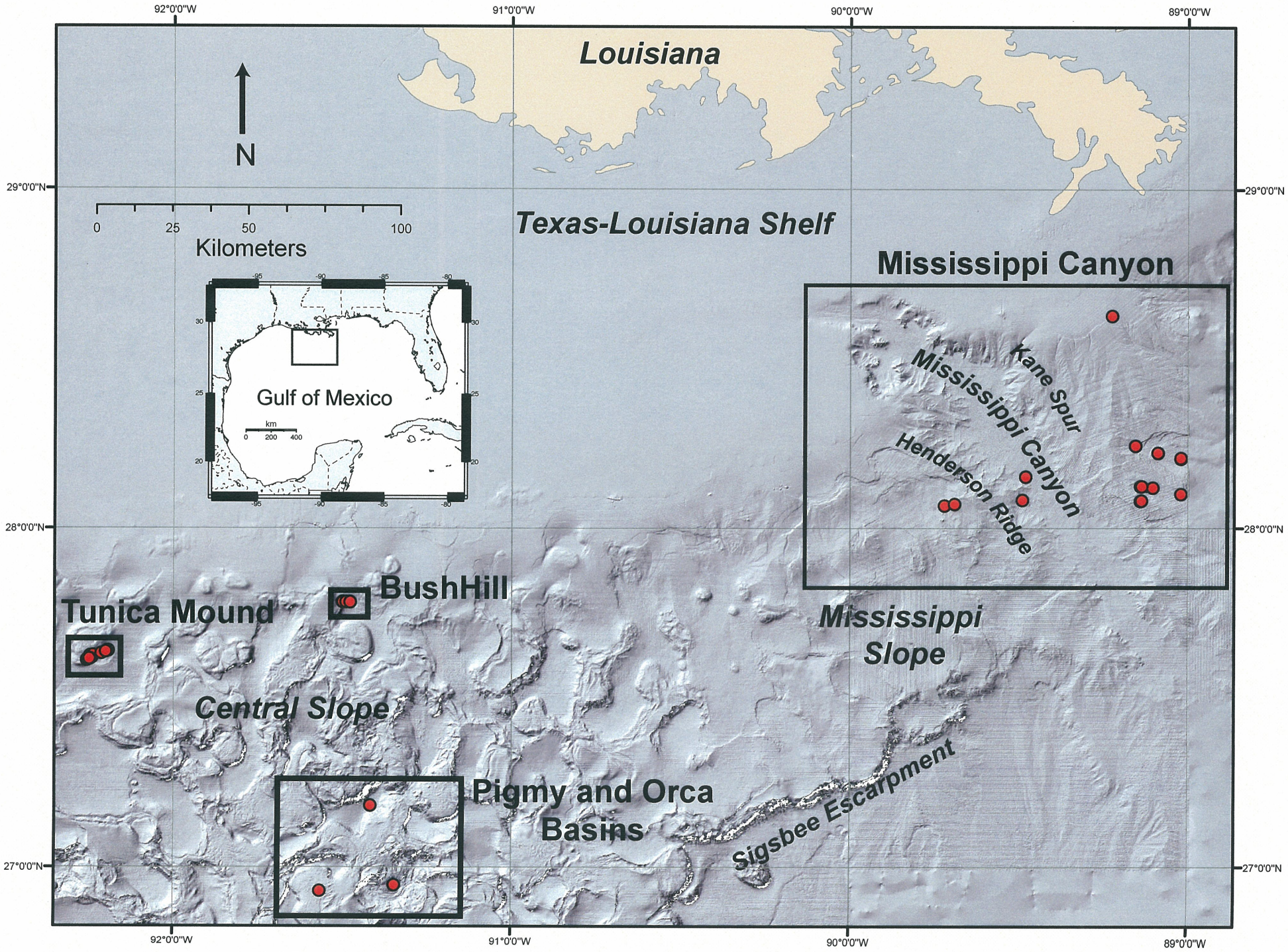
92°0'0"W
91°0'0"W
90°0'0"W
89°0'0"W
29°0'0"N
28°0'0"N
27°0'0"N
Louisiana
N
0 25 50 100
Kilometers
Texas-Louisiana Shelf
Gulf of Mexico
km
0 200 400
Mississippi Canyon
Kane Spur
Mississippi Canyon
Henderson Ridge
BushHill
Tunica Mound
Mississippi Slope
Central Slope
Pigmy and Orca Basins
Sigsbee Escarpment

Hydrocarbon Gases from Giant Piston Cores in the Northern Gulf of Mexico: Results from the IMAGES VIII/PAGE 127 cruise of the RV Marion Dufresne, July, 2002

Thomas D. Lorenson[1]
Jennifer A. Dougherty[1]
James G. Flocks[2]

[1]U.S. Geological Survey, 345 Middlefield Rd., MS-999, Menlo Park, California 94025 (tlorenson@usgs.gov)
[2]U.S. Geological Survey, 600 4th Street S., St. Petersburg, Florida 33701

Hydrocarbon Gases from Giant Piston Cores in the Northern Gulf of Mexico: Results from the IMAGES VIII/PAGE 127 cruise of the RV Marion Dufresne, July, 2002; chapter 9 in Winters, W.J., Lorenson, T.D., Paull, C.K., eds., 2005, Initial report of the IMAGES VIII/PAGE 127 gas hydrate and paleoclimate cruise on the RV *Marion Dufresne in the Gulf of Mexico, 2-18 July 2002, U.S. Geological Survey Open-File Report 2004-1358.*

Abstract

Hydrocarbon gases and carbon dioxide (CO_2) extracted from sediment cores from the northern Gulf of Mexico in four distinct regions were studied to constrain the possible occurrence and source of gas that may form gas hydrate. Three sample types were analyzed; gas from dissociated gas hydrate, dissolved gas in sediment, and free gas evolved from sediment collected from gas voids in the core liner.

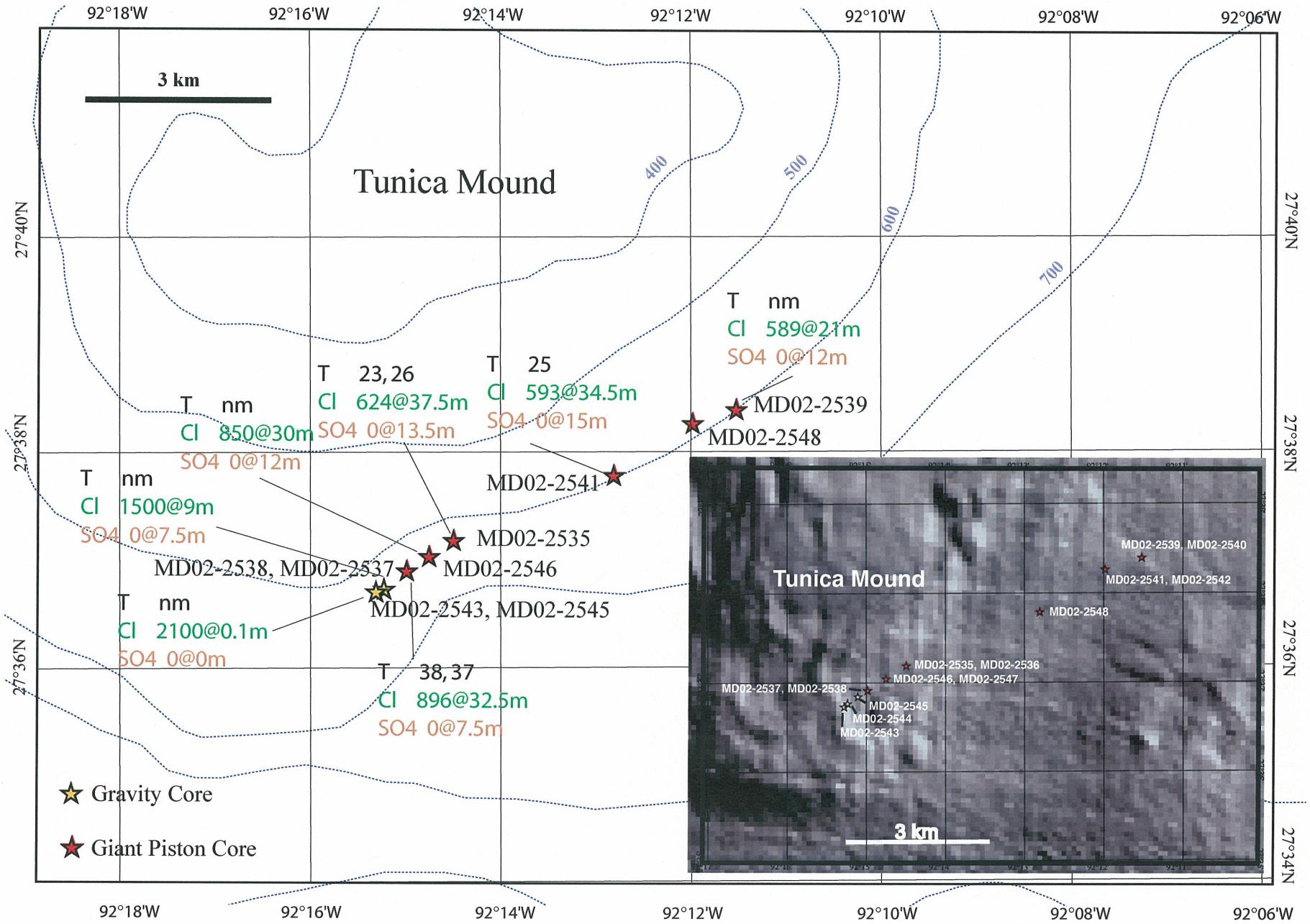

Figure 2. Cores sites adjacent to Tunica Mound. Gravity and giant piston cores noted with yellow and red stars respectively. Other core observations indicated as follows. T = measured geothermal gradient (degrees C/km); Cl = chloride ion concentration (mM) maximum at the corresponding depth (mbsf); and SO4 = sulfate ion concentration (mM) minimum at the corresponding depth (mbsf) indication the depth to the sulfate-methane interface (SMI).

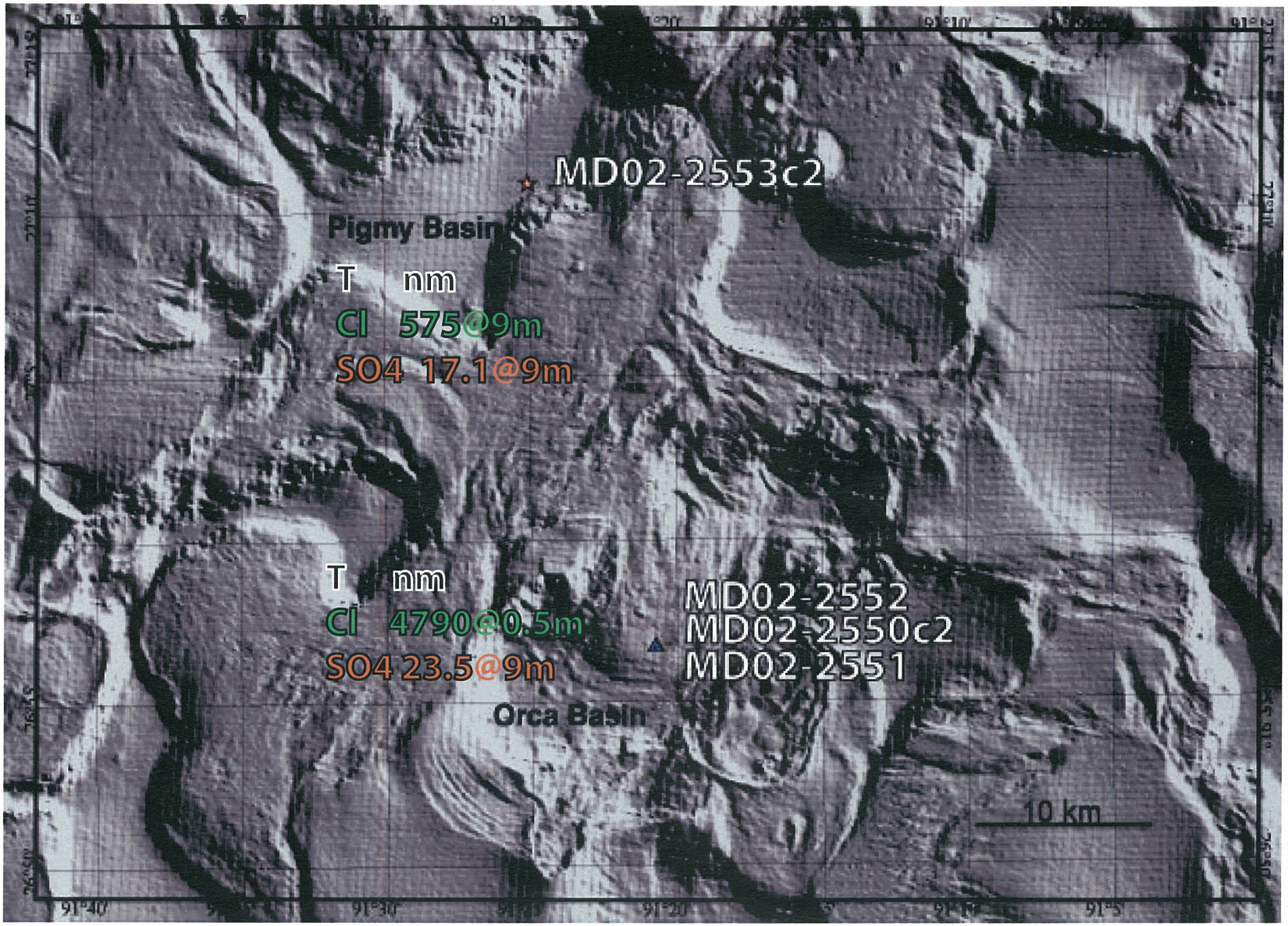

Figure 3. Cores sites adjacent to Tunica Mound. Gravity and giant piston cores noted with yellow and red stars respectively. Other core observations indicated as follows. T = measured geothermal gradient (degrees C/km); Cl = chloride ion concentration (mM) maximum at the corresponding depth (mbsf); and SO4 = sulfate ion concentration (mM) minimum at the corresponding depth (mbsf) indication the depth to the sulfate-methane interface (SMI).

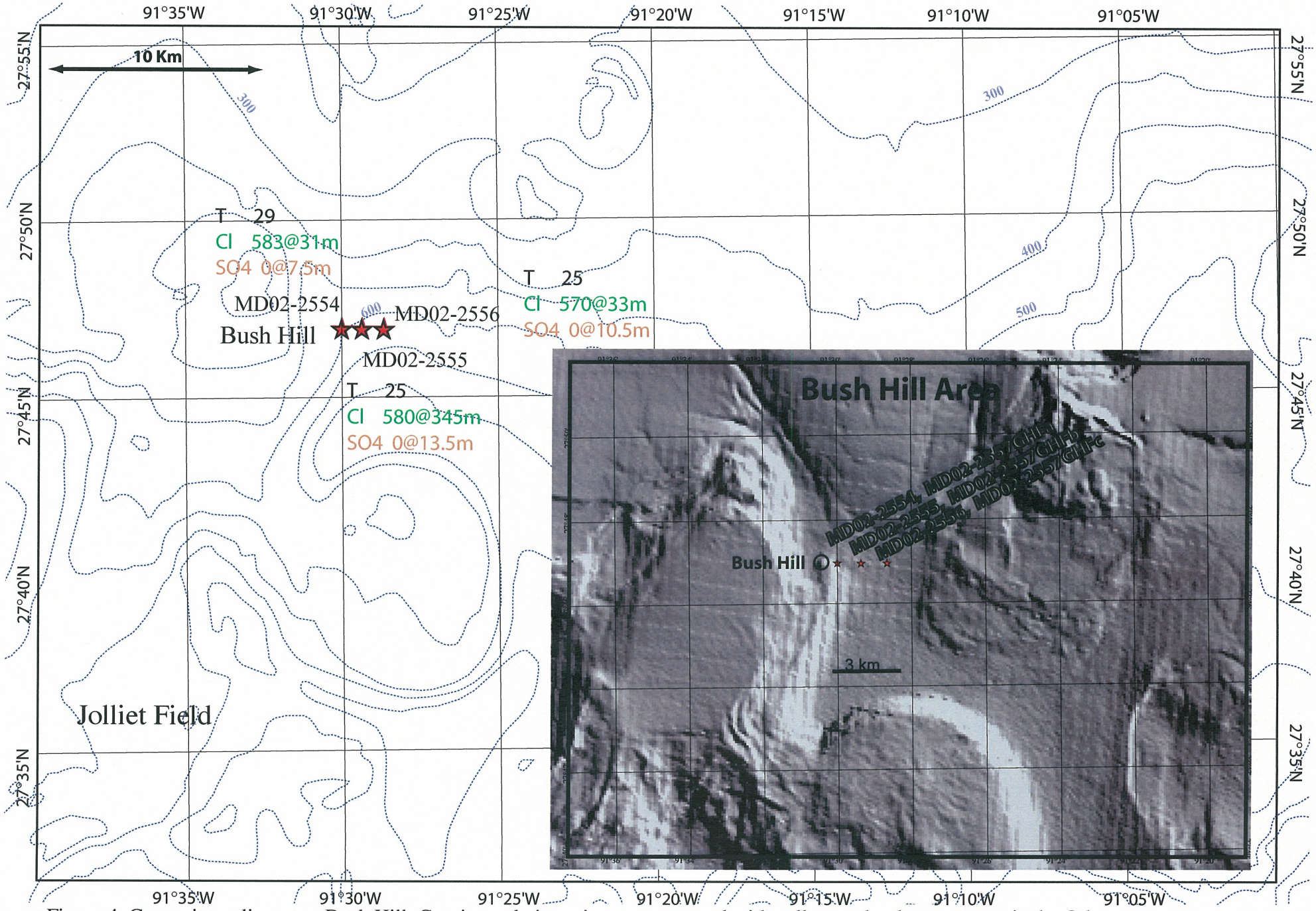

Figure 4. Cores sites adjacent to Bush Hill. Gravity and giant piston cores noted with yellow and red stars respectively. Other core observations indicated as follows. T = measured geothermal gradient (degrees C/km); Cl = chloride ion concentration (mM) maximum at the corresponding depth (mbsf); and SO4 = sulfate ion concentration (mM) minimum at the corresponding depth (mbsf) indication the depth to the sulfate-methane interface (SMI).

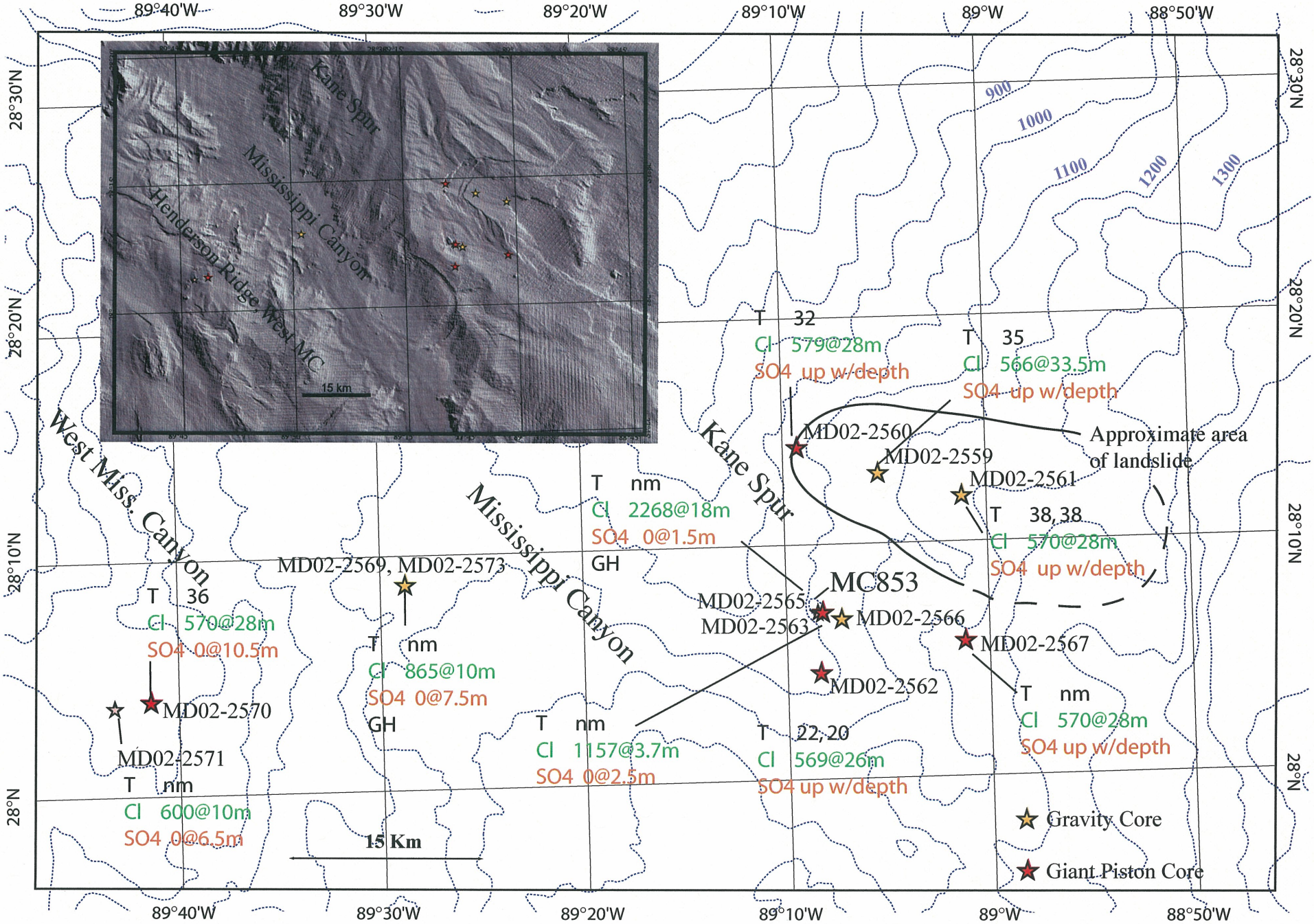

Figure 5. Cores sites in the Mississippi Canyon region. Contours in meters. Gravity and giant piston cores noted with yellow and red stars respectively. Other core observations indicated as follows. T = measured geothermal gradient (degrees C/km), nm+ not measured; Cl = chloride ion concentration (mM) maximum at the corresponding depth (mbsf); and SO4 = sulfate ion concentration (mM) minimum at the corresponding depth (mbsf) indication the depth to the sulfate-methane interface (SMI), up w/depth = SO4 concentration increases with depth.

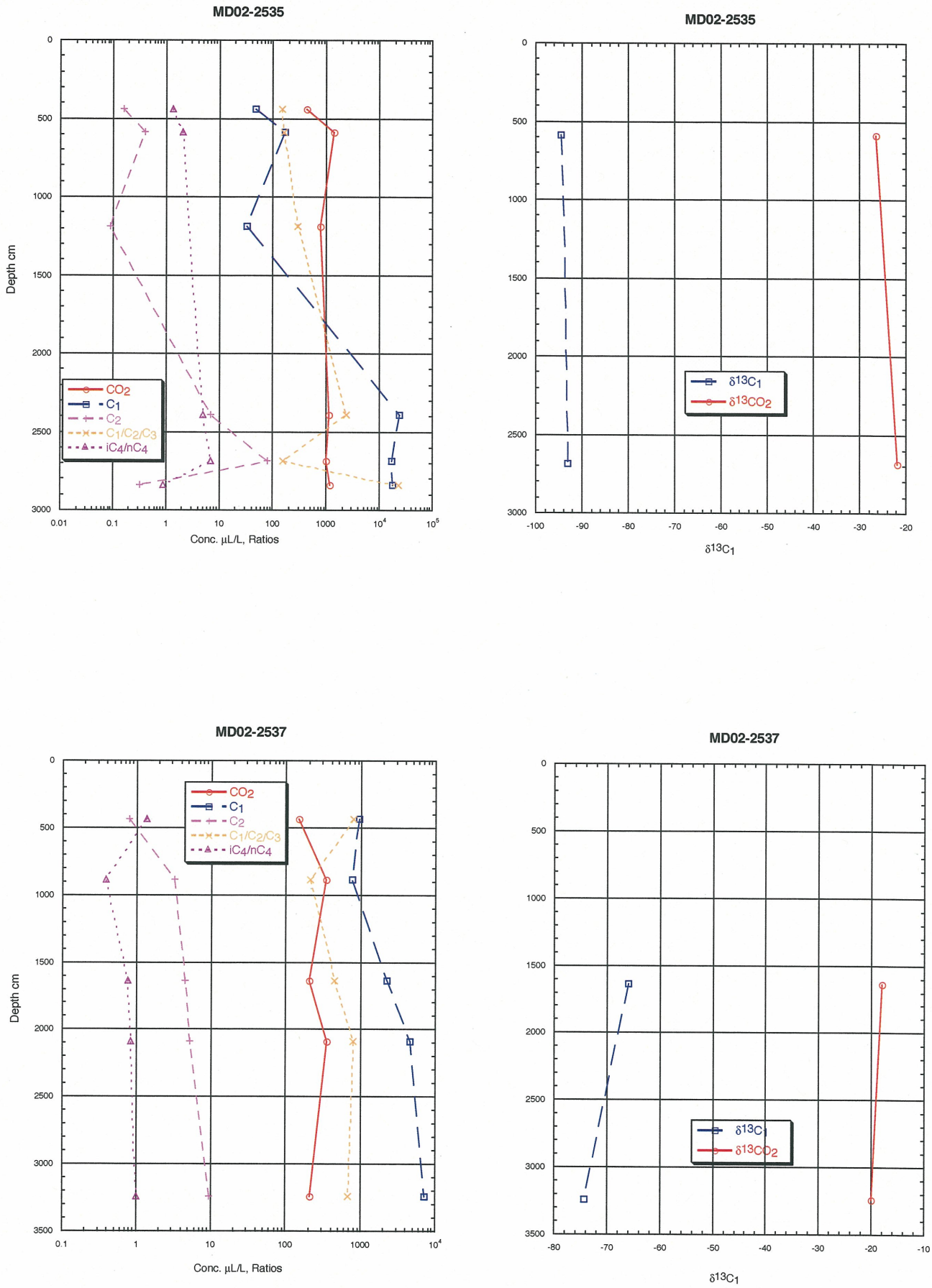
MD02-2535
Depth cm
Conc. µL/L, Ratios
CO2
C1
C2
C1/C2/C3
iC4/nC4
MD02-2535
δ13C1
δ13CO2
MD02-2537
Depth cm
Conc. µL/L, Ratios
CO2
C1
C2
C1/C2/C3
iC4/nC4
MD02-2537
δ13C1
δ13CO2

Figure 6

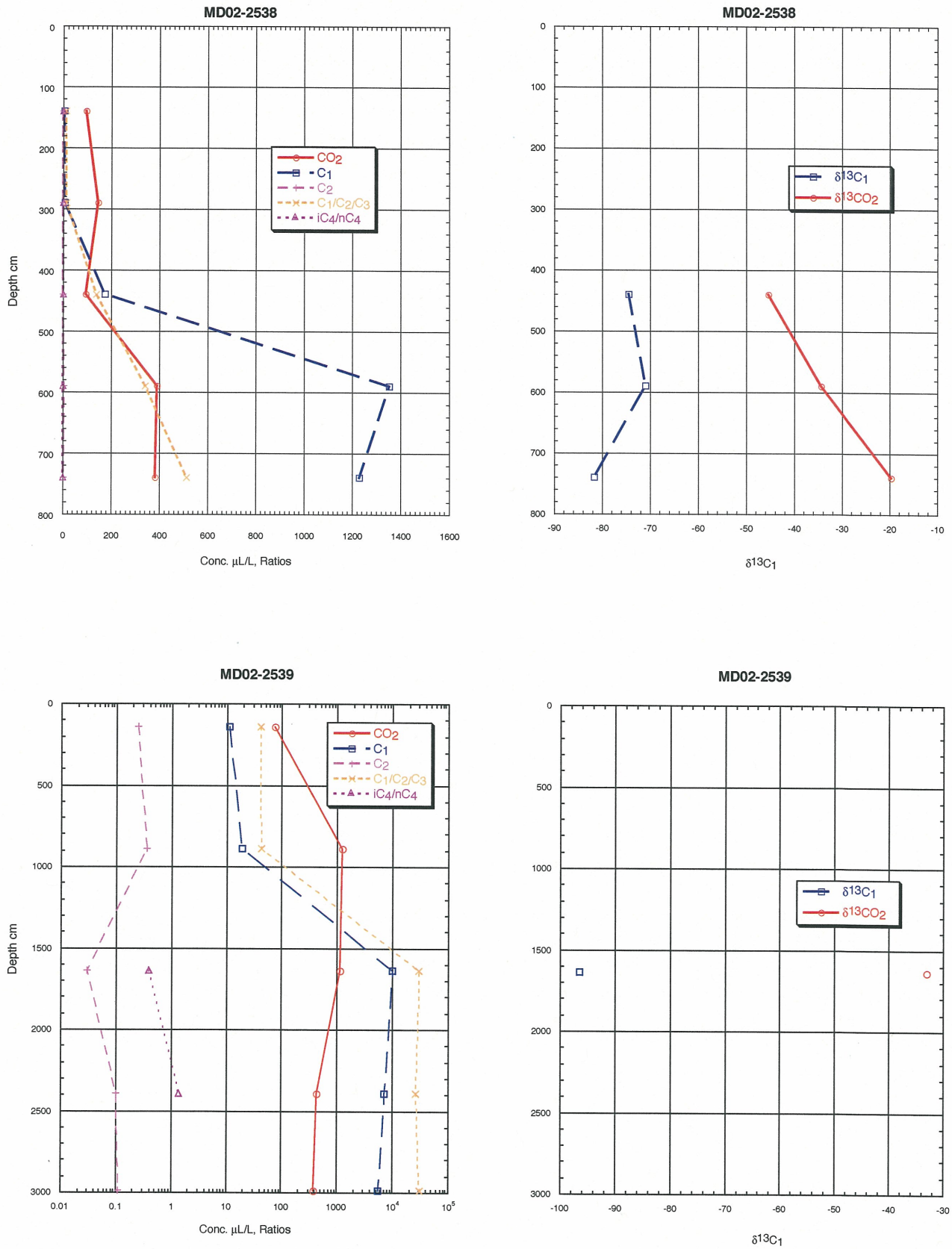
MD02-2538
Depth cm
Conc. µL/L, Ratios
CO2
C1
C2
C1/C2/C3
iC4/nC4
MD02-2538
δ13C1
δ13CO2
MD02-2539
Depth cm
Conc. µL/L, Ratios
CO2
C1
C2
C1/C2/C3
iC4/nC4
MD02-2539
δ13C1
δ13CO2

Figure 7

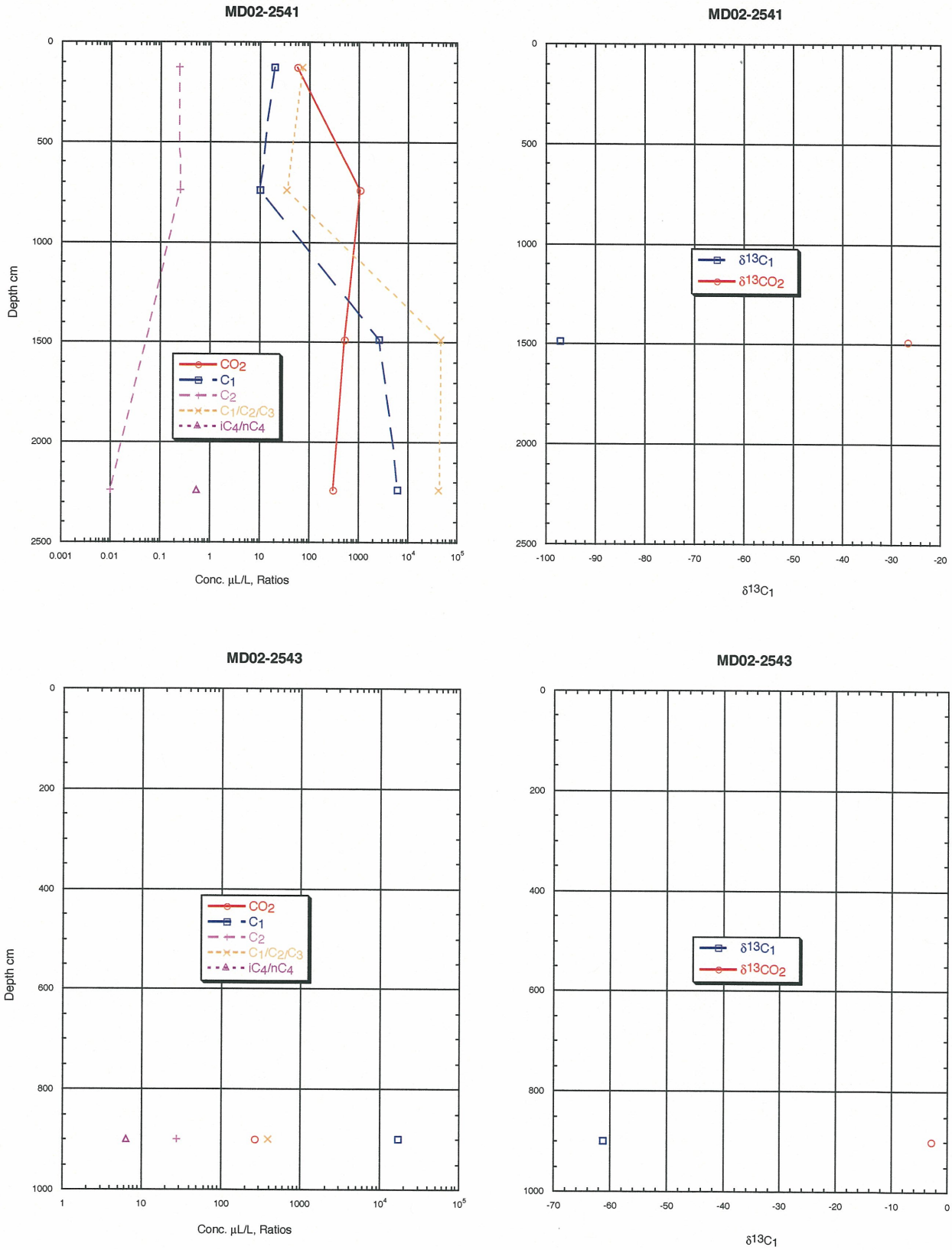
MD02-2541
Depth cm
Conc. µL/L, Ratios
CO2
C1
C2
C1/C2/C3
iC4/nC4
MD02-2541
δ13C1
δ13CO2
MD02-2543
Depth cm
Conc. µL/L, Ratios
CO2
C1
C2
C1/C2/C3
iC4/nC4
MD02-2543
δ13C1
δ13CO2

Figure 8

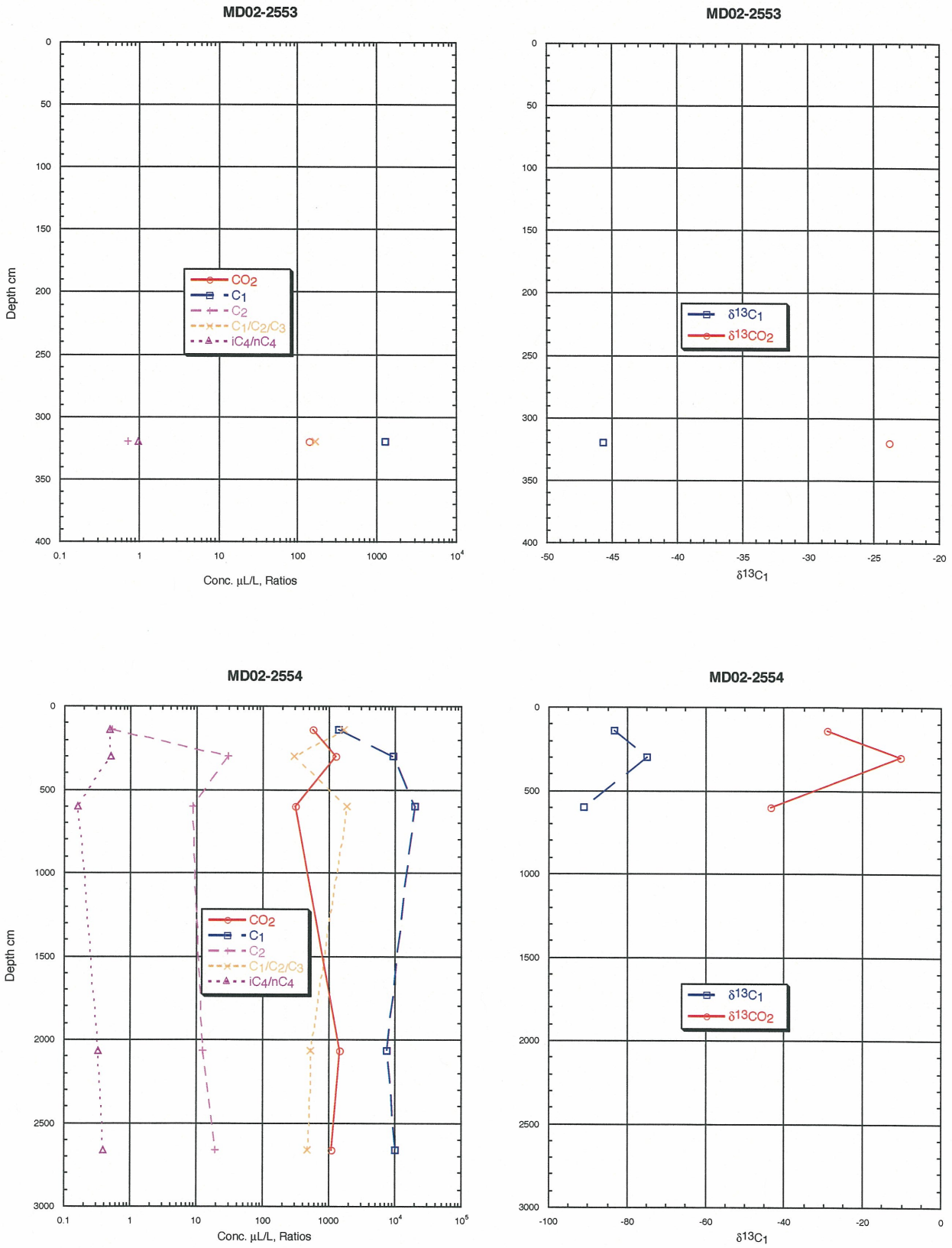
MD02-2553
Depth cm
Conc. µL/L, Ratios
CO2
C1
C2
C1/C2/C3
iC4/nC4
MD02-2553
δ13C1
δ13CO2
MD02-2554
Depth cm
Conc. µL/L, Ratios
CO2
C1
C2
C1/C2/C3
iC4/nC4
MD02-2554
δ13C1
δ13CO2

Figure 9

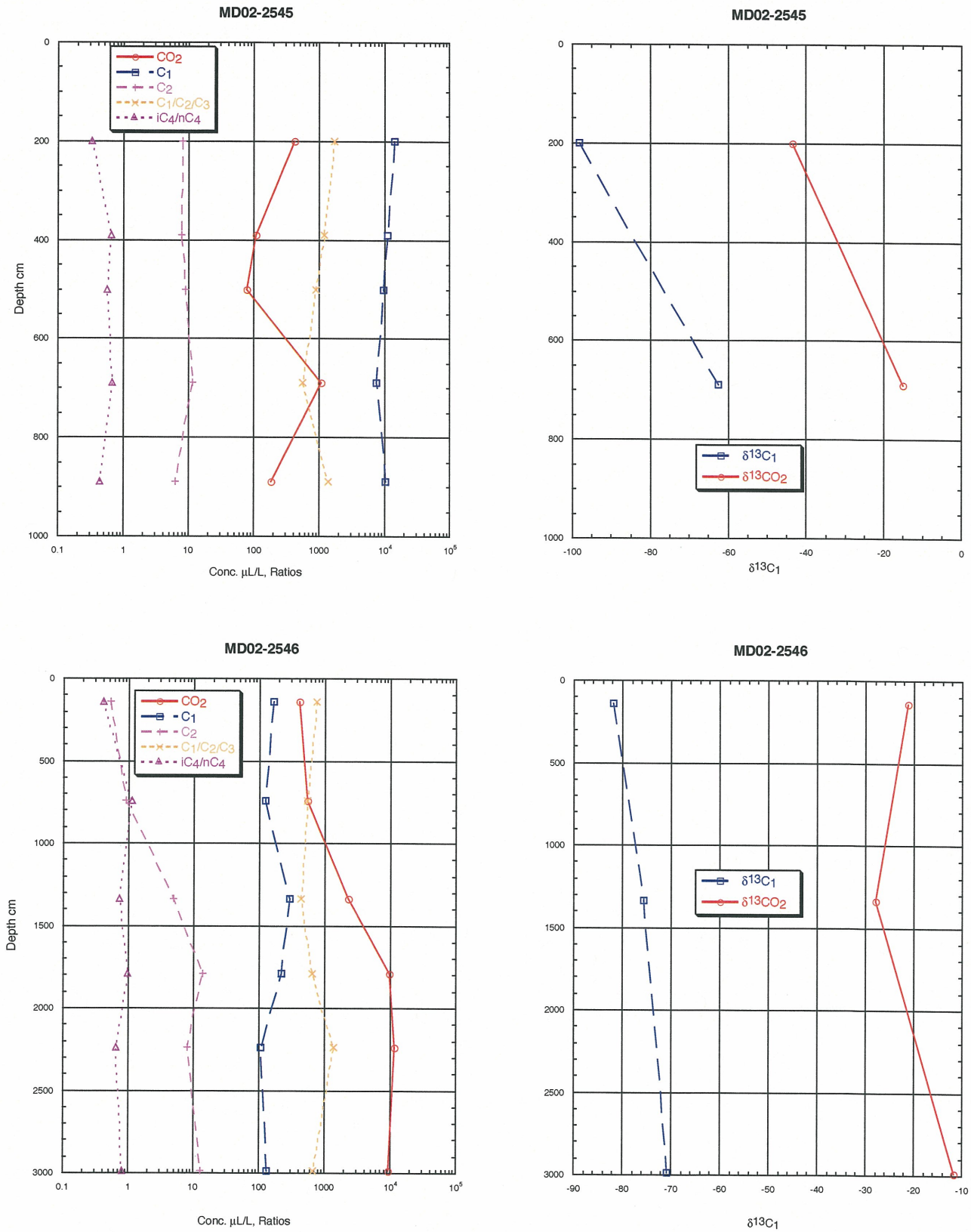
MD02-2545
CO2
C1
C2
C1/C2/C3
iC4/nC4
Depth cm
Conc. µL/L, Ratios
MD02-2545
δ13C1
δ13CO2
δ13C1
MD02-2546
CO2
C1
C2
C1/C2/C3
iC4/nC4
Depth cm
Conc. µL/L, Ratios
MD02-2546
δ13C1
δ13CO2
δ13C1

Figure 10

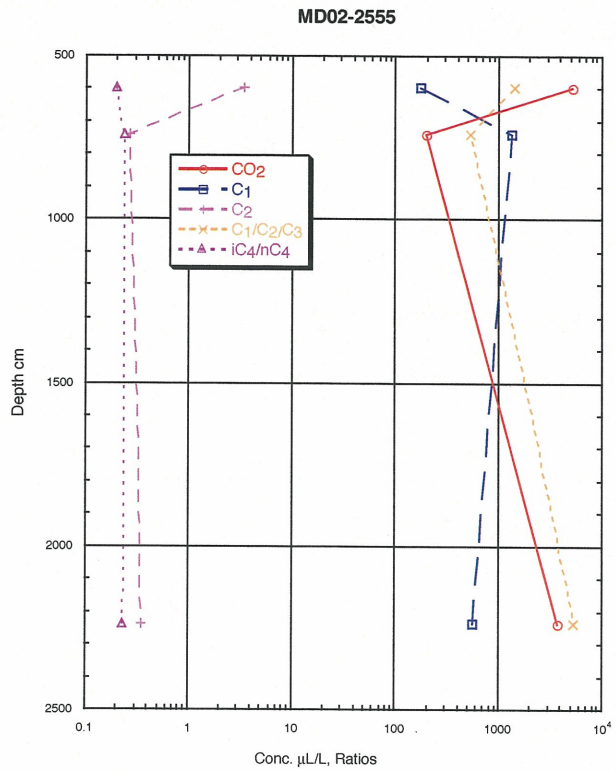

No Isotope data

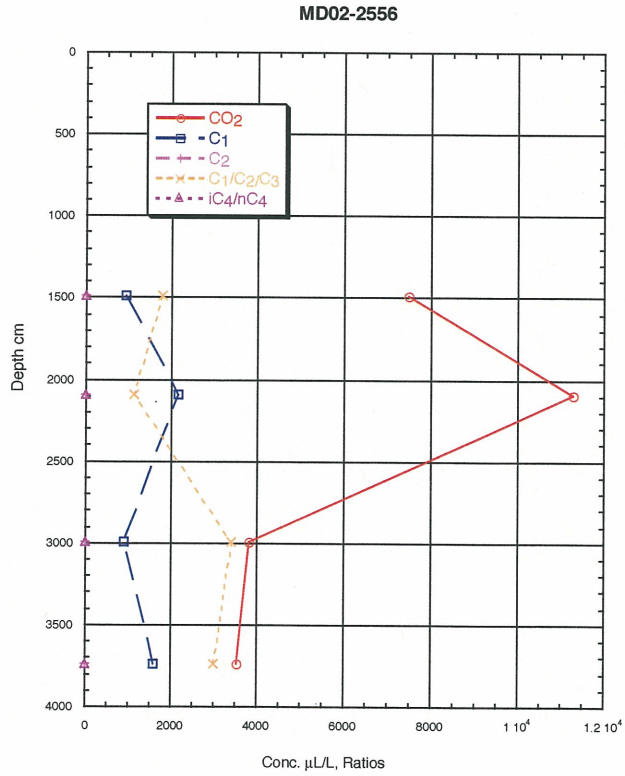

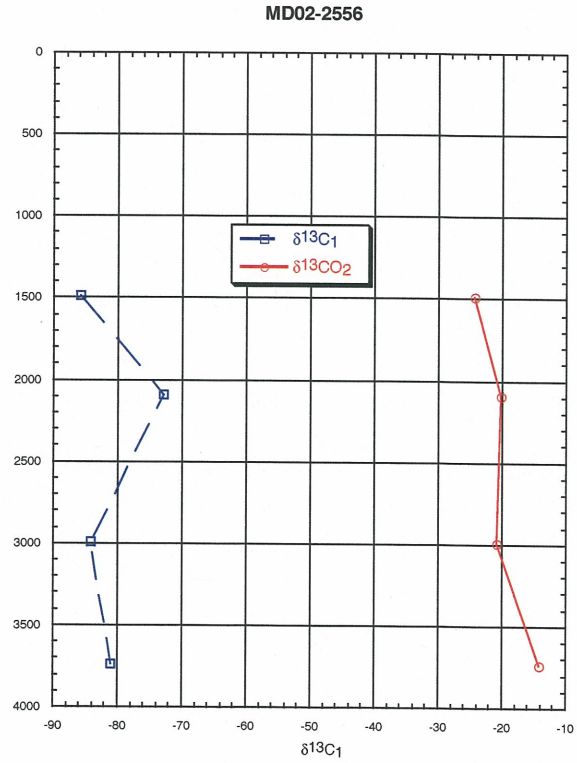

Figure 11

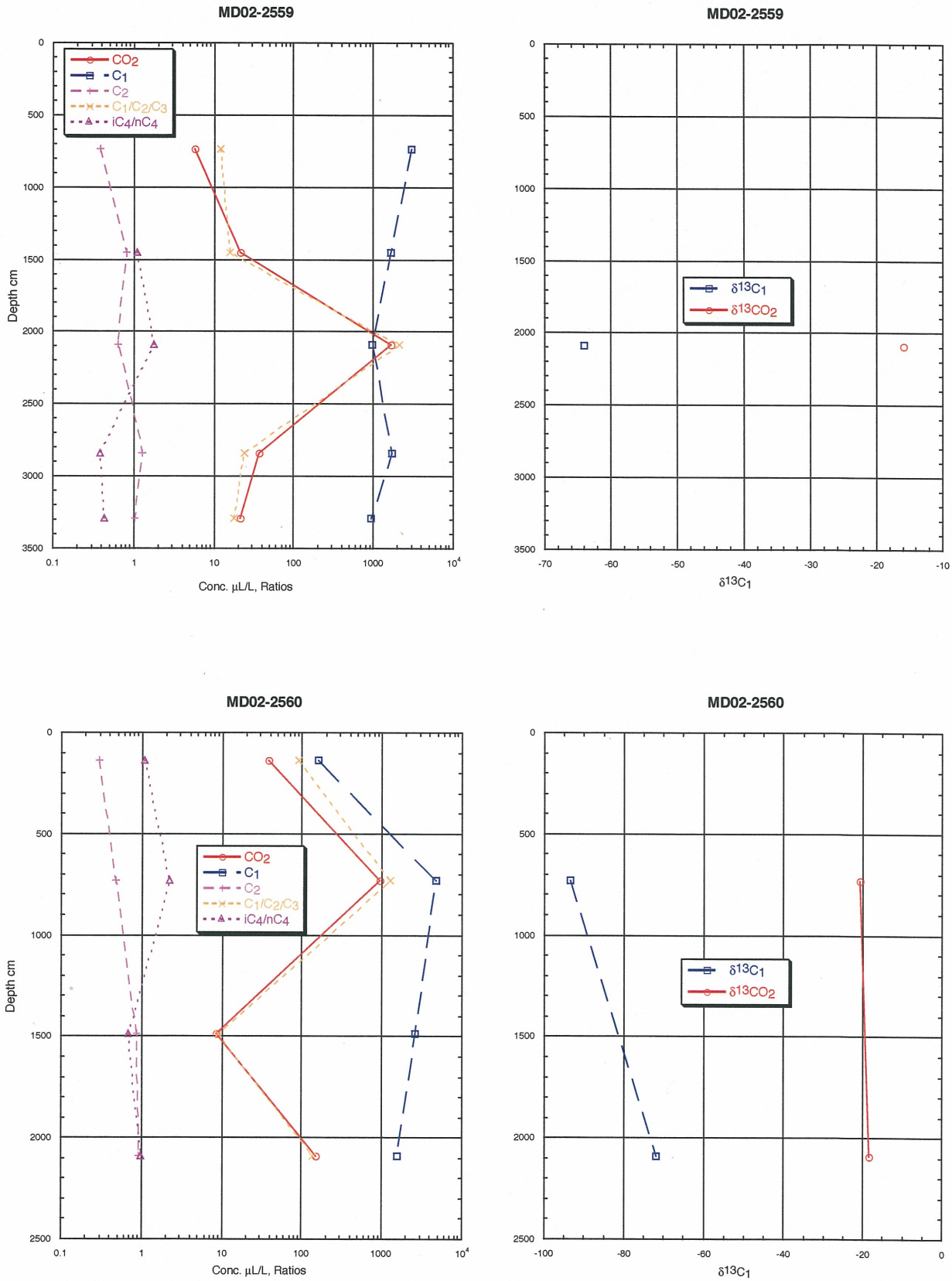
MD02-2559
CO2
C1
C2
C1/C2/C3
iC4/nC4
Depth cm
Conc. µL/L, Ratios
MD02-2559
δ13C1
δ13CO2
δ13C1
MD02-2560
CO2
C1
C2
C1/C2/C3
iC4/nC4
Depth cm
Conc. µL/L, Ratios
MD02-2560
δ13C1
δ13CO2
δ13C1

Figure 12

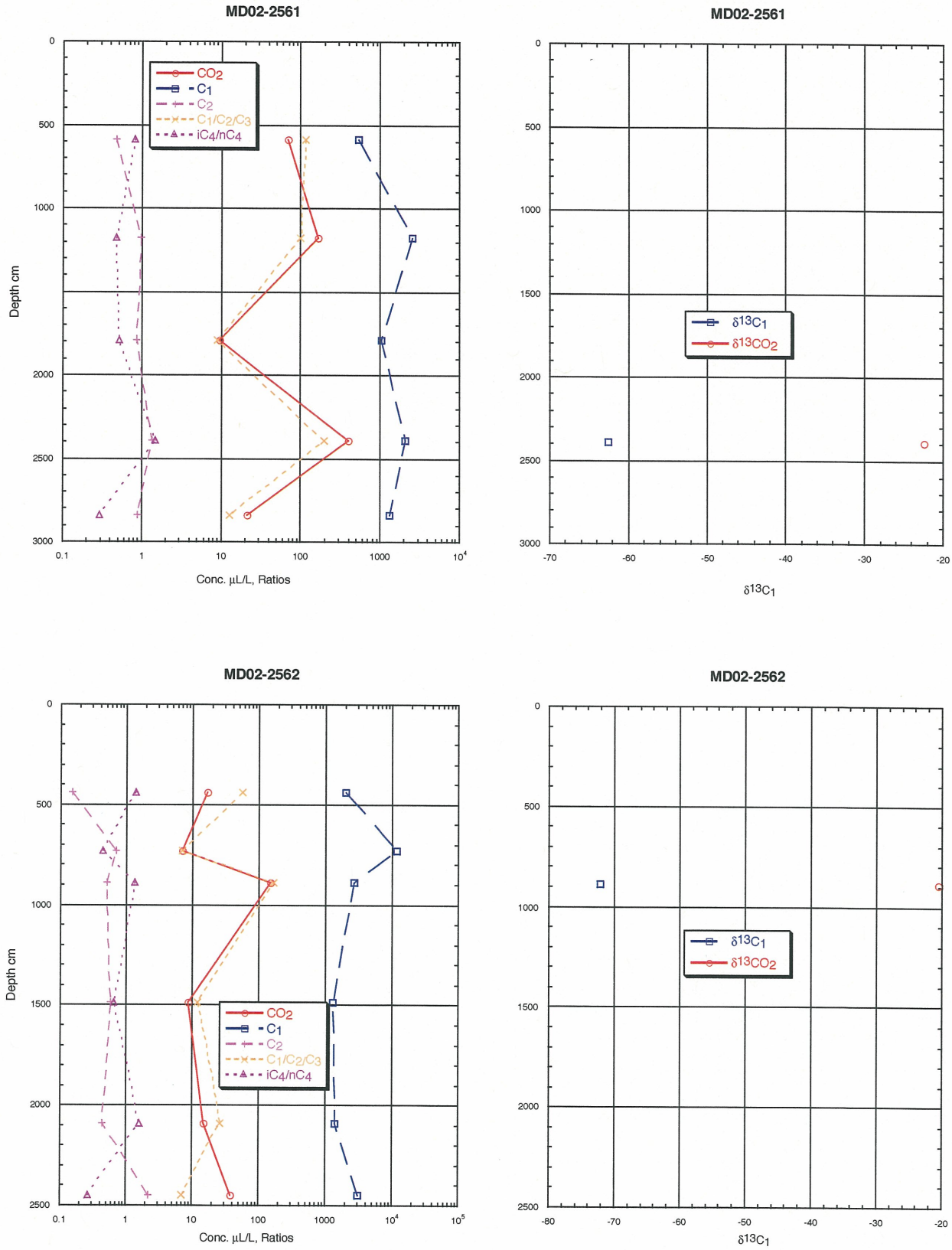
MD02-2561
CO2
C1
C2
C1/C2/C3
iC4/nC4
Depth cm
Conc. µL/L, Ratios
MD02-2561
δ13C1
δ13CO2
δ13C1
MD02-2562
CO2
C1
C2
C1/C2/C3
iC4/nC4
Depth cm
Conc. µL/L, Ratios
MD02-2562
δ13C1
δ13CO2
δ13C1

Figure 13

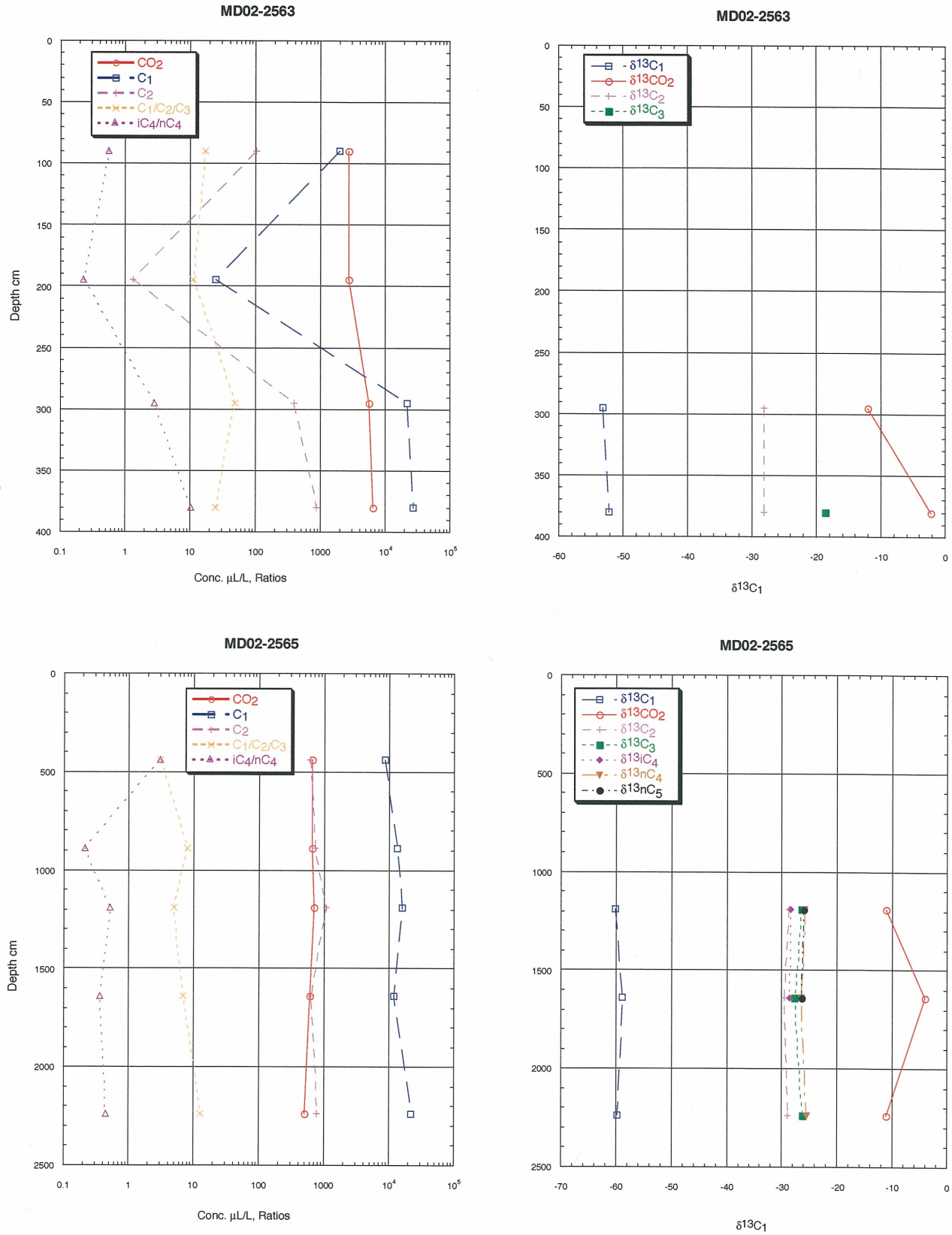
MD02-2563
CO2
C1
C2
C1/C2/C3
iC4/nC4
Depth cm
Conc. µL/L, Ratios
MD02-2563
δ13C1
δ13CO2
δ13C2
δ13C3
δ13C1
MD02-2565
CO2
C1
C2
C1/C2/C3
iC4/nC4
Depth cm
Conc. µL/L, Ratios
MD02-2565
δ13C1
δ13CO2
δ13C2
δ13C3
δ13iC4
δ13nC4
δ13nC5
δ13C1

Figure 14

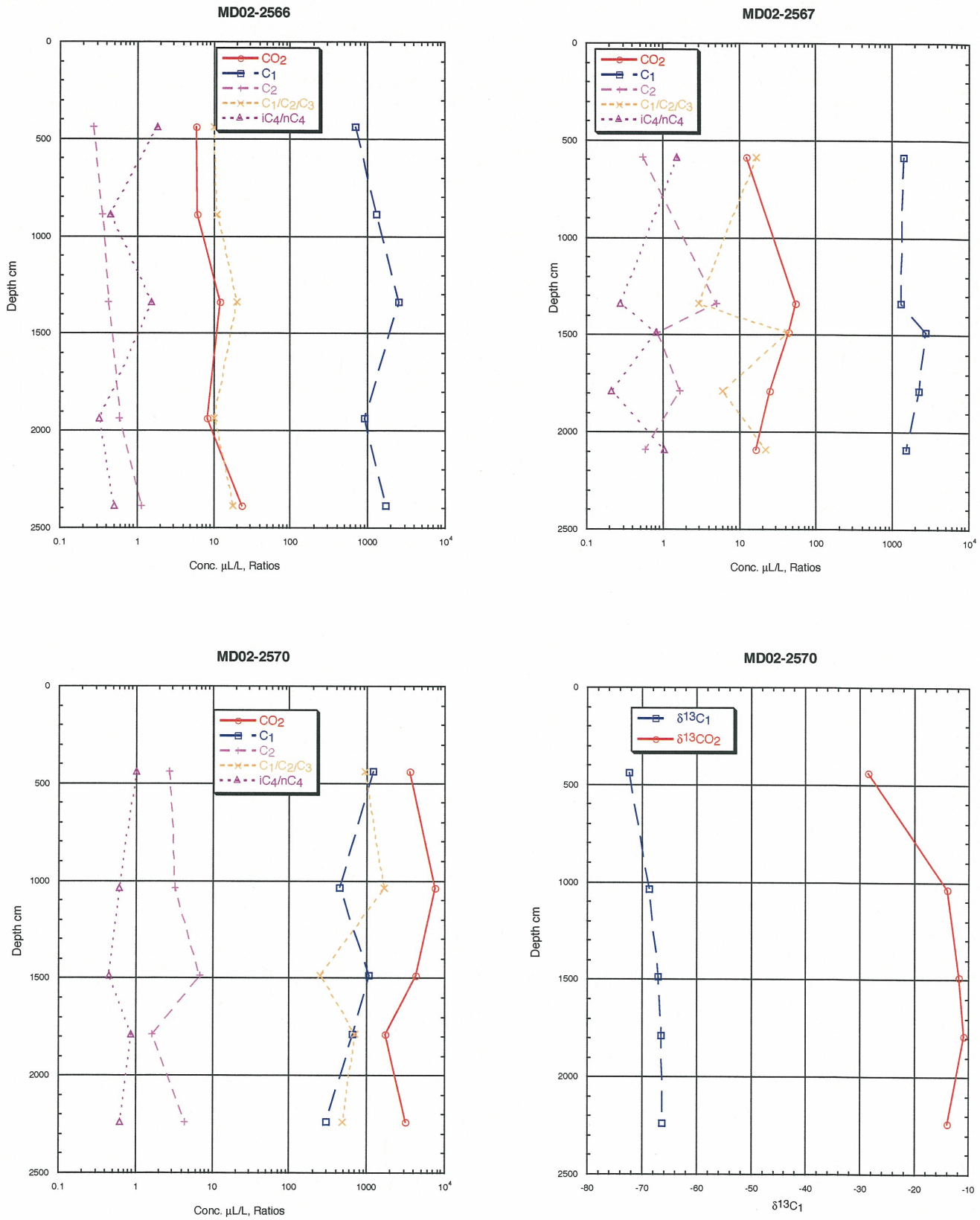
MD02-2566
MD02-2567
MD02-2570
MD02-2570
CO2
C1
C2
C1/C2/C3
iC4/nC4
δ13C1
δ13CO2
Depth cm
Conc. µL/L, Ratios
δ13C1

Figure 15

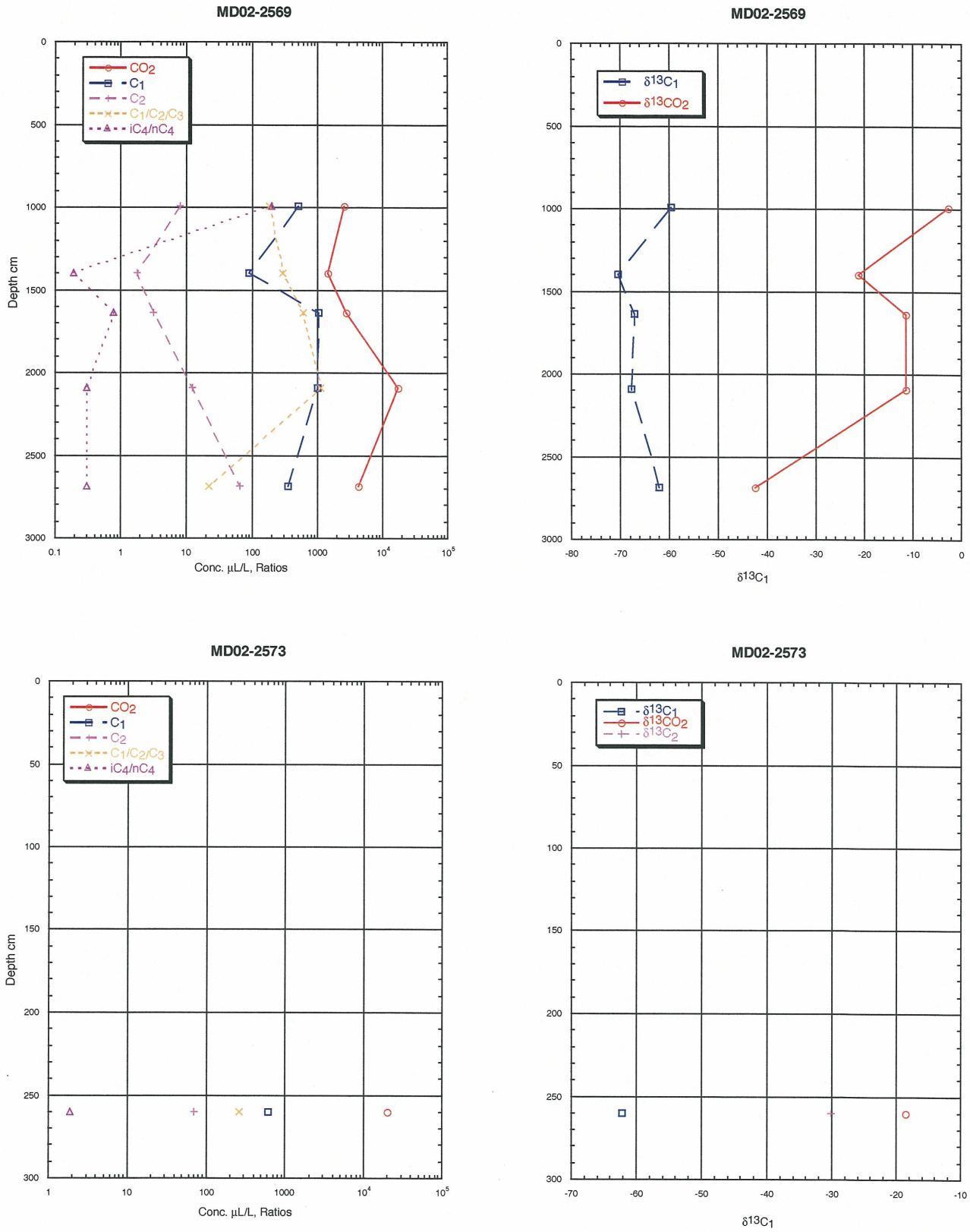
MD02-2569
CO2
C1
C2
C1/C2/C3
iC4/nC4
Depth cm
Conc. µL/L, Ratios
MD02-2569
δ13C1
δ13CO2
δ13C1
MD02-2573
CO2
C1
C2
C1/C2/C3
iC4/nC4
Depth cm
Conc. µL/L, Ratios
MD02-2573
δ13C1
δ13CO2
δ13C2
δ13C1

Figure 16

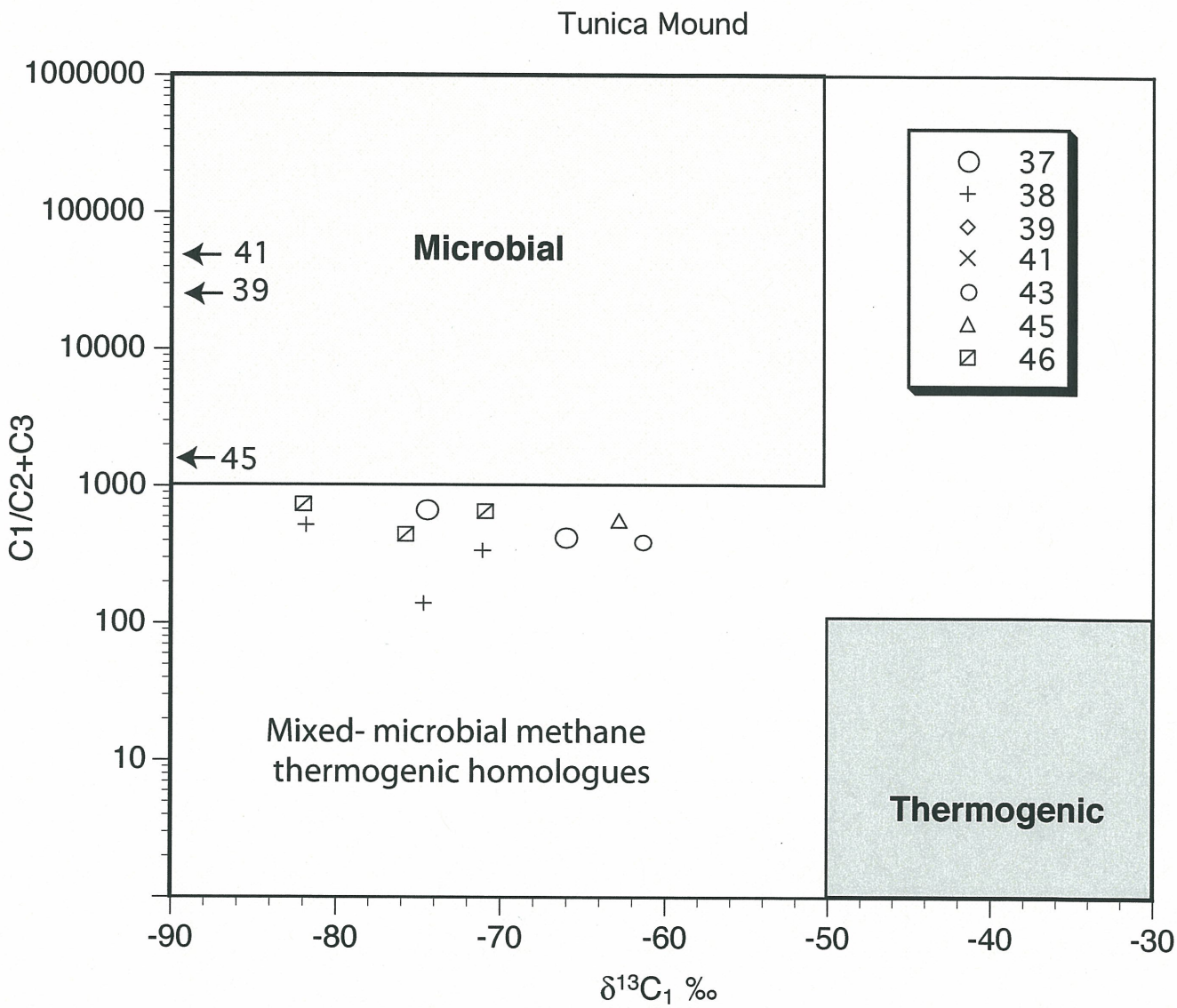

Figure 17. Plot of methane carbon isotopic composition versus the gas wetness ratio C1/C2+C3 for Tunica Mound core gas. Primary fields representing accepted values for microbial and thermogenic sourced methane gas are noted. Carbon isotopic compositions less than -90 ppt. are not plotted but are noted by core number with relative gas wetness ratios indicated by position on the y-axis.

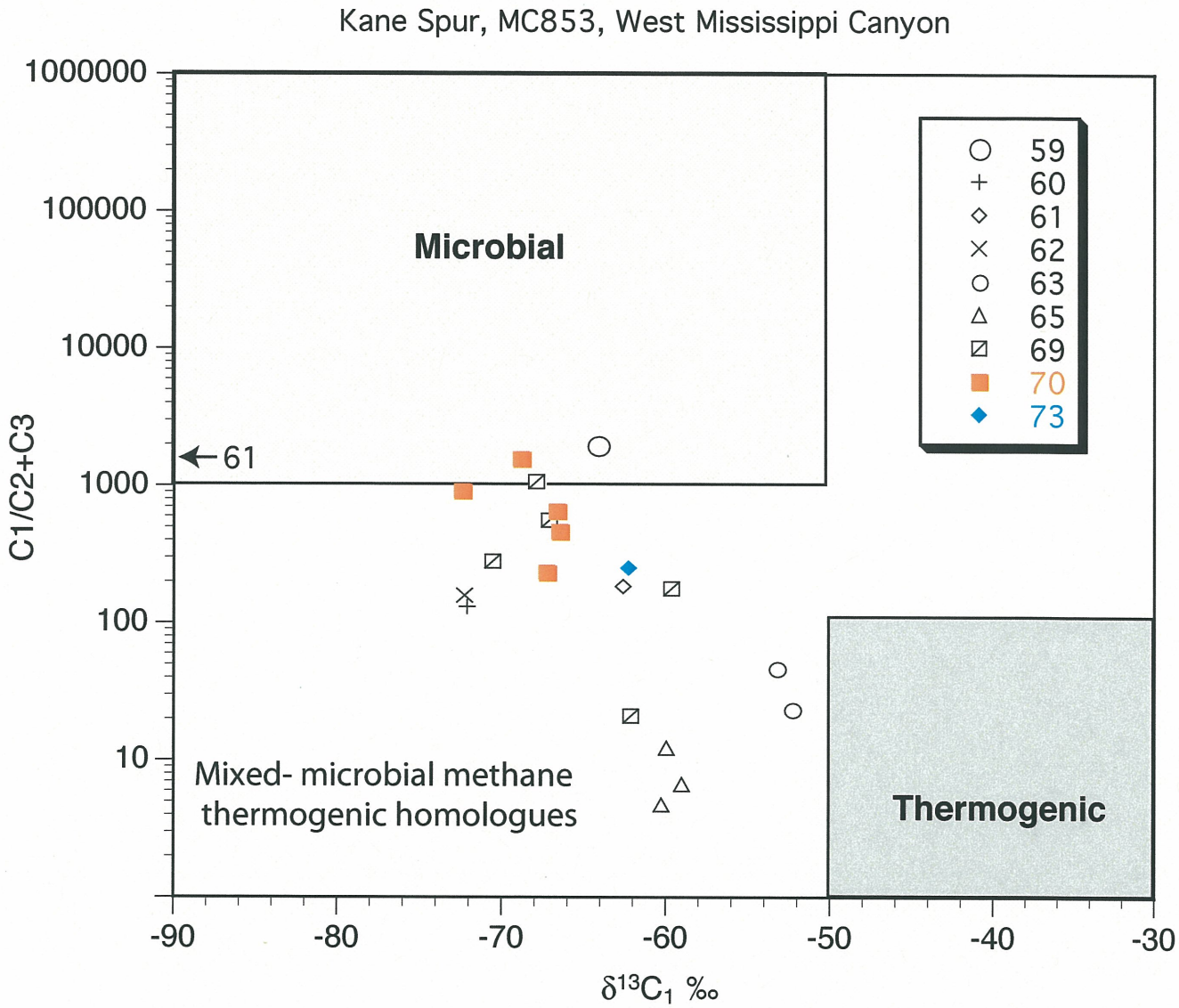

Figure 18. Plot of methane carbon isotopic composition versus the gas wetness ratio C1/C2+C3 for Kane Spur (59, 60, 61, and 62), MC853 (63 and 65), and West Mississippi Canyon (69, 70, and 73) core gas. Primary fields representing accepted values for microbial and thermogenic sourced methane gas are noted. Carbon isotopic compositions less than -90 ppt are not plotted but are noted by core number with relative gas wetness ratios indicated by position on the y-axis.